

Time-dependent quantum geometric tensor and some applications

Bogar Díaz^{1,2}, Diego Gonzalez^{3,4}, Marcos J. Hernández¹, and J. David Vergara¹

¹ Departamento de Física de Altas Energías, Instituto de Ciencias Nucleares, Universidad Nacional Autónoma de México, Apartado Postal 70-543, Ciudad de México, 04510, México

² Group of Biometrics, Biosignals, Security and Smart Mobility (GB2S), Department of Mathematics Applied to Information and Communication Technologies, Universidad Politécnica de Madrid, Avda. Complutense, 30, 28040 Madrid, Spain

³ Escuela Superior de Ingeniería Mecánica y Eléctrica, Instituto Politécnico Nacional, Unidad Profesional Adolfo López Mateos, Zacatenco, 07738 Gustavo A. Madero, Ciudad de México, México

⁴ Departamento de Física, Cinvestav, Avenida Instituto Politécnico Nacional 2508, San Pedro Zacatenco, 07360 Gustavo A. Madero, Ciudad de México, México

E-mail: bogar.diaz@upm.es, dgonzalezv@ipn.mx, mhm@ciencias.unam.mx, vergara@nucleares.unam.mx

Abstract. We define a time-dependent extension of the quantum geometric tensor to describe the geometry of the time-parameter space for a quantum state, by considering small variations in both time and wave function parameters. Compared to the standard quantum geometric tensor, this tensor introduces new temporal components, enabling the analysis of systems with non-time-separable or explicitly time-dependent quantum states and encoding new information about these systems. In particular, the time-time component of this tensor is related to the energy dispersion of the system. We applied this framework to a harmonic/inverted oscillator, a time-dependent harmonic oscillator, and a chain of generalized harmonic/inverted oscillators. We show some results on the scalar curvature associated with the time-dependent quantum geometric tensor and the generalized Berry curvature behavior on the transition from harmonic oscillators to inverted ones. Furthermore, we analyze the entanglement for the chain through purity analysis, obtaining that the purity for any excited state is zero in the mentioned transitions.

1. Introduction

The geometrical description of quantum phenomena has led to significant results in physics. Notably, Pancharatnam's work on polarized light interference [1] laid the foundation for understanding geometric phases. Independently, Berry [2] and Simon [3] showed that the Berry phase is a holonomy in a Hermitian line bundle, within the context of an adiabatic evolution. After that, these works were extended to consider

non-adiabatic cases by Aharonov and Anandan [4, 5], while Samuel and Bhandari [6, 7] generalized them further to non-cyclic and non-unitary evolutions. Anandan and Aharonov [8] approached the problem geometrically, showing that the energy uncertainty integral corresponds to the distance along a curve measured by the Fubini-Study metric. Subsequently, the work of Provost and Valle [9] on the construction of the quantum geometric tensor (QGT) allowed them to give an utterly geometrical structure to the parameter space of a quantum system. Following the ideas of Provost and Valle, it has been shown that the geometry of the parameter space encodes much of the relevant quantum information of a system, such as the identification of phase transitions [10–13], along with non-equilibrium steady-state quantum phase transitions [14, 15] and the excited state quantum phase transitions [16, 17].

In this work, we extend and unify the previous developments by considering a non-adiabatic evolution and a manifold constructed out of the parameters and the system’s time dependence. In this way, we carry out a covariant construction of the QGT, a time-dependent quantum geometric tensor (tQGT), in the sense that we consider the parameters and time on the same foot. This is analogous to a relativistic space-time description, but with a Euclidean signature. A notable feature of our formalism is that in the case of stationary states, the temporal components of the tQGT are zero, and our development is directly reduced to the QGT of Provost and Valle [9]. We find that the Berry curvature is generalized, called tBerry curvature, and acquires time components containing non-trivial information about the system and can be thought of as the components of an “electric field”. This allows to obtain information from the system that can not be obtained in any other way. This is illustrated through the harmonic oscillator, where the tQGT enables us to identify the ground state of the system, corresponding to the place where the time-parameter components of the tBerry curvature change sign or the time-parameter components of the generalized metric become zero. The tQGT also allows us to identify the transition from a harmonic oscillator to an inverted harmonic oscillator. In addition, whether the energy of the inverted oscillator is greater than zero or less than zero.

This paper is organized as follows. In Sec. 2, we introduce the tQGT (Q_{IJ}) and divide it into real and imaginary parts. The real part of the new tensor defines a time-dependent quantum metric that generalizes the quantum metric tensor, while its imaginary part generalizes the Berry curvature. We show that the tQGT is gauge invariant under time-dependent gauge transformations and that the time-time component (Q_{00}) corresponds to the energy dispersion. Furthermore, we prove that the tQGT reduces to the standard QGT for stationary states. Section 3 introduces our first example, the harmonic and inverted oscillators. Both systems are studied using Gaussian solutions that are non-separable on time, allowing us to give a unified description. We analyze the general case of these solutions and built the tQGT, showing what information can be obtained. We also study in detail the transition zone between harmonic and inverted, displaying that the tQGT diverges at the transition point. Section 4 contains an example of a system with a time-dependent Hamiltonian. To

be precise, we study the tQGT for a time-dependent harmonic oscillator. In Sec. 5 we extend the results of Sec. 3 to a system of coupled particles. Furthermore, considering several degrees of freedom and the fact that our states are Gaussian, we also compute and analyze the purity of the quantum system of coupled particles. We pay special attention to the transition zone, where we show that the purity of the reduced system is zero for all even excited eigenstates. Finally, we give our conclusions in Sec. 6.

2. Time-dependent quantum geometric tensor

In this section, we introduce a tQGT. We begin by considering a system, defined by a Hamiltonian operator \hat{H} , in a quantum state at time t , represented by a normalized state $|\Psi(t; \lambda)\rangle$ with a set of parameters $\lambda = \{\lambda^i\}$ ($i, j, \dots = 1, \dots, \mathcal{N}$). We assume that time and parameters are independent quantities, and then consider a full set of time and parameters denoted by $\Lambda = \{\Lambda^I\} = \{\Lambda^0, \Lambda^i\}$ ($I, J, \dots = 0, 1, \dots, \mathcal{N}$) with $\Lambda^0 = t$ and $\Lambda^i = \lambda^i$. Using this notation, we can write the state of the system as $|\Psi(\Lambda)\rangle := |\Psi(t; \lambda)\rangle$. Notice that, in general, the Hamiltonian can be time-dependent and can depend on the parameters λ , but not necessarily all of them.

Let us now introduce an infinitesimal displacement $\Lambda \rightarrow \Lambda' = \Lambda + \delta\Lambda$, and the corresponding ket state at Λ' , which we denote as $|\Psi(\Lambda + \delta\Lambda)\rangle$. The distance between the states $|\Psi(\Lambda)\rangle$ and $|\Psi(\Lambda + \delta\Lambda)\rangle$ is defined by

$$dl^2 \equiv 1 - |\langle \Psi(\Lambda) | \Psi(\Lambda + \delta\Lambda) \rangle|^2, \quad (1)$$

where $|\langle \Psi(\Lambda) | \Psi(\Lambda + \delta\Lambda) \rangle|$ is recognized as the fidelity.

Expanding the state $|\Psi(\Lambda + \delta\Lambda)\rangle$ into a second-order Taylor series, we have

$$|\Psi(\Lambda + \delta\Lambda)\rangle \simeq |\Psi(\Lambda)\rangle + \sum_{I=0}^{\mathcal{N}} |\partial_I \Psi(\Lambda)\rangle \delta\Lambda^I + \frac{1}{2} \sum_{I,J=0}^{\mathcal{N}} |\partial_I \partial_J \Psi(\Lambda)\rangle \delta\Lambda^I \delta\Lambda^J, \quad (2)$$

where $\partial_I \equiv \frac{\partial}{\partial \Lambda^I}$. Using (2), it is straightforward to see that the distance (1) can be expressed as

$$dl^2 \simeq \sum_{I,J=0}^{\mathcal{N}} g_{IJ}(\Lambda) \delta\Lambda^I \delta\Lambda^J, \quad (3)$$

where we designate the time-dependent quantum metric tensor (tQMT) as

$$g_{IJ}(\Lambda) := \text{Re}(Q_{IJ}(\Lambda)), \quad (4)$$

which is the real part of the Hermitian tensor

$$Q_{IJ}(\Lambda) := \langle \partial_I \Psi(\Lambda) | \partial_J \Psi(\Lambda) \rangle - \langle \partial_I \Psi(\Lambda) | \Psi(\Lambda) \rangle \langle \Psi(\Lambda) | \partial_J \Psi(\Lambda) \rangle. \quad (5)$$

We define $Q_{IJ}(\Lambda)$ as the tQGT and it can be regarded as a generalization of the standard QGT, as it includes new components associated with the time index ($I = 0$), specifically Q_{00} , Q_{0i} and Q_{i0} . Furthermore, an important feature of the tensor $Q_{IJ}(\Lambda)$ is that it

provides new and nontrivial information when $|\Psi(\Lambda)\rangle$ is not separable in time. On the other hand, the tQMT, $g_{IJ}(\Lambda)$, plays a fundamental role in describing the geometrical aspects of the parameter space, since it allows the measurement of the distance between the nearby states $|\Psi(\Lambda)\rangle$ and $|\Psi(\Lambda + \delta\Lambda)\rangle$ in the time parameter manifold \mathcal{M} .

The tensor $Q_{IJ}(\Lambda)$ is in general complex, and its imaginary part can be associated with a 2-form time-dependent curvature $F = \frac{1}{2} \sum_{I,J=0}^{\mathcal{N}} F_{IJ} \delta\Lambda^I \wedge \delta\Lambda^J$ with components

$$F_{IJ}(\Lambda) = -2\text{Im}(Q_{IJ}(\Lambda)). \quad (6)$$

Further, these components can be written as $F_{IJ}(\Lambda) = \partial_I A_J(\Lambda) - \partial_J A_I(\Lambda)$, where $A_I(\Lambda)$ are the time-dependent connection coefficients

$$A_I(\Lambda) = -\text{Im}(\langle \Psi(\Lambda) | \partial_I \Psi(\Lambda) \rangle). \quad (7)$$

It is clear that (7) can be thought of as a generalization of the Berry connection [2]. For this reason, we call F the tBerry curvature.

On the other hand, it is not hard to show that under the gauge transformation

$$|\Psi(\Lambda)\rangle \rightarrow |\Psi'(\Lambda)\rangle = \exp(i\alpha(\Lambda)) |\Psi(\Lambda)\rangle, \quad (8)$$

where $\alpha(\Lambda)$ is an arbitrary real function of time and parameters, the tQGT $Q_{IJ}(\Lambda)$ is gauge-invariant, i.e.,

$$Q_{IJ}(\Lambda) \rightarrow Q'_{IJ}(\Lambda) = Q_{IJ}(\Lambda), \quad (9)$$

while the time-dependent connection $A_I(\Lambda)$ transforms as

$$A_I(\Lambda) \rightarrow A'_I(\Lambda) = A_I(\Lambda) - \partial_I \alpha(\Lambda), \quad (10)$$

i.e., $A_I(\Lambda)$ is gauge-dependent.

It worth noting that assuming the time evolution of $|\Psi(\Lambda)\rangle$ is determined by the Schrödinger equation, $\hat{H}|\Psi(\Lambda)\rangle = i\hbar|\partial_0\Psi(\Lambda)\rangle$, the temporal component of (5) becomes

$$\begin{aligned} Q_{00}(\Lambda) &= \frac{1}{\hbar^2} \left(\langle \Psi(\Lambda) | \hat{H}^2 | \Psi(\Lambda) \rangle - \langle \Psi(\Lambda) | \hat{H} | \Psi(\Lambda) \rangle^2 \right) \\ &= \frac{(\Delta E)^2}{\hbar^2}, \end{aligned} \quad (11)$$

where $(\Delta E)^2$ is the energy dispersion. Equation (11) reproduces the result obtained by Anandan and Aharonov in [18], where only the infinitesimal time displacement $t \rightarrow t' = t + \delta t$ is taken into account. Notice that because of (11), for a stationary state

$$|\Psi(\Lambda)\rangle = \exp\left(-\frac{iE_n(\lambda)}{\hbar}t\right) |n(\lambda)\rangle, \quad (12)$$

where $|n(\lambda)\rangle$ satisfy the eigenvalues equation $\hat{H}|n(\lambda)\rangle = E_n(\lambda)|n(\lambda)\rangle$ with nondegenerate eigenvalue $E_n(\lambda)$, the component $Q_{00}(\Lambda)$ vanishes, as expected. In fact, in this case, the only non-vanishing components of (5) are the parameter components

$$Q_{ij}(\lambda) = \langle \partial_i n(\lambda) | \partial_j n(\lambda) \rangle - \langle \partial_i n(\lambda) | n(\lambda) \rangle \langle n(\lambda) | \partial_j n(\lambda) \rangle, \quad (13)$$

which do not depend on time and can be recognized as the components of the standard QGT [9].

In what follows, we explore the consequences of (5) by considering general quantum states that are not stationary.

3. Harmonic oscillator and inverted harmonic oscillator

Along this paper, we work with solutions of the time-dependent Schrödinger equation that are non-time-separable. In the case of one dimension, we consider the family of Gaussian solutions of the form

$$\psi(q, \Lambda) = C(\Lambda)e^{-(U(\Lambda)+iV(\Lambda))q^2/2}, \quad (14)$$

where $U(\Lambda) > 0$, $V(\Lambda) \in \mathbb{R}$, and $C(\Lambda) \in \mathbb{C}$. We remember that $\Lambda = \{t, \lambda^i\}$. Hereafter, we use $\hbar = 1$. The normalization condition on (14) implies

$$|C(\Lambda)|^2 = \sqrt{\frac{U(\Lambda)}{\pi}}. \quad (15)$$

Using the approach introduced in Section 2 for the calculation of the tQGT and taking the real part, we find that the tQMT components (4) are given by

$$g_{IJ} = \frac{\partial_I U \partial_J U + \partial_I V \partial_J V}{8U^2}. \quad (16)$$

On the other hand, taking the imaginary part, we find that the components of the tBerry curvature (6) correspond to

$$F_{IJ} = \frac{-\partial_I U \partial_J V + \partial_I V \partial_J U}{4U^2}. \quad (17)$$

For this model, the determinant of the metric is zero if $\mathcal{N} > 2$, which implies that only two elements Λ^I can be independent. Therefore, in the following, we will only consider the metrics obtained by varying any two selected elements, Λ^{I_1} and Λ^{I_2} , while keeping the rest fixed. We denote this metric by $\tilde{\mathbf{g}}[\Lambda^{I_1}, \Lambda^{I_2}]$, explicitly, it is given by

$$\tilde{\mathbf{g}}[\Lambda^{I_1}, \Lambda^{I_2}] = \begin{pmatrix} g_{I_1 I_1} & g_{I_1 I_2} \\ g_{I_1 I_2} & g_{I_2 I_2} \end{pmatrix}. \quad (18)$$

All these metrics, for any two selected parameters, satisfy the Palumbo and Goldman relation [19], which was first observed in the context of the dimensional reduction in [20, 21]. Specifically, the relation is $\det \tilde{\mathbf{g}}[\Lambda^{I_1}, \Lambda^{I_2}] = (F_{I_1 I_2})^2$, with I_1 and I_2 fixed. On the other hand, the scalar curvature for any of these metrics is denoted by $\mathcal{R}[\Lambda^{I_1}, \Lambda^{I_2}]$ and satisfies $\mathcal{R}[\Lambda^{I_1}, \Lambda^{I_2}] = -16$ if $\det \tilde{\mathbf{g}}[\Lambda^{I_1}, \Lambda^{I_2}] \neq 0$, otherwise it cannot be calculated. This means that the 2-dimensional time-parameter space of these Gaussian

states possess a hyperbolic geometry. These properties of the metric for systems with wave function (14) are summarized in the following set of equations

$$\det \mathbf{g} = 0, \quad \text{if } \mathcal{N} > 2, \quad (19a)$$

$$\det \tilde{\mathbf{g}}[\Lambda^{I_1}, \Lambda^{I_2}] = \frac{1}{4} (F_{I_1 I_2})^2, \quad \text{if } \mathcal{N} = 2, \quad (19b)$$

$$\mathcal{R}[\Lambda^{I_1}, \Lambda^{I_2}] = -16, \quad \text{if } \mathcal{N} = 2 \text{ and } \det \tilde{\mathbf{g}}[\Lambda^{I_1}, \Lambda^{I_2}] \neq 0. \quad (19c)$$

A system that admits this kind of solution is

$$\hat{H}(\hat{q}, \hat{p}, \Lambda) = \frac{1}{2} (W\hat{p}^2 + X\hat{q}^2), \quad (20)$$

where $W > 0$ and $X \in \mathbb{R}$. Notice that this system presents a bifurcation at $X = 0$. From the classical point of view, for $X > 0$, the system corresponds to the simple harmonic oscillator, where we have an elliptical stable fixed point at $(p, q) = (0, 0)$. On the other hand, for $X < 0$, the system represents an inverted harmonic oscillator, with a hyperbolic unstable fixed point at $(p, q) = (0, 0)$. We refer to $X > 0$ and $X < 0$ as regions 1 and 2, respectively. The simple and the inverted harmonic oscillators conserve energy, making them integrable. From a quantum point of view, the case $X > 0$ has normalizable and time-separable solutions, given by the well-known Hermite functions. However, for $X < 0$, such solutions do not exist [22]. To obtain normalizable solutions, it is possible to follow two strategies: confine the system as in [23] or consider solutions that are non-time-separable as in [24]. For our purposes, the latter is more convenient and the one we will follow in this work. Notably, this type of solution also exists for the case of $X > 0$, as seen in [25].

In what follows, we consider the cases $X > 0$ and $X < 0$ separately, and then we compare the information obtained from the two systems and analyze the transition of the two regions. The idea is to start in both regions with an initial state at $t = 0$,

$$\psi(q, 0; \lambda) = \left(\frac{B\sqrt{|XW|}}{W\pi} \right)^{1/4} \exp \left(-\frac{\sqrt{|XW|}Bq^2}{2W} \right), \quad (21)$$

where $\{\lambda^i\} = \{X, W, B\}$, with $i = 1, 2, 3$ and $B > 0$. Later, we evolve this initial state over time with the system's kernel. We then analyze the resulting wave functions using the tQGT to see what information we observe from the system.

3.1. Region 1: harmonic oscillator

In this case, the kernel of the system is given by

$$K(q', t; q, 0) = \sqrt{\frac{\omega}{2\pi i W t}} \exp \left(-\frac{\omega((q^2 + q'^2) \cos(\omega t) - 2qq')}{2iW \sin(\omega t)} \right), \quad (22)$$

where $\omega = \sqrt{XW}$. Using (22), the wave packet (21) takes the form

$$\psi_{HO}(q, t; \lambda) = \left(\frac{B\omega}{W\pi}\right)^{1/4} \frac{1}{\sqrt{\cos(\omega t) + iB \sin(\omega t)}} \exp\left(-\frac{q^2 \omega (1 - iB \cot(\omega t))}{2W(B - i \cot(\omega t))}\right). \quad (23)$$

This is a particular case of the wave function (14), where the functions $U(\Lambda)$, $V(\Lambda)$ and $C(\Lambda)$ are given by

$$U_{HO}(\Lambda) = \frac{BX \csc^2(\omega t)}{\omega (B^2 + \cot^2(\omega t))}, \quad (24a)$$

$$V_{HO}(\Lambda) = \frac{(B^2 - 1) X \cot(\omega t)}{\omega (B^2 + \cot^2(\omega t))}, \quad (24b)$$

$$C_{HO}(\Lambda) = \left(\frac{B\omega}{W\pi}\right)^{1/4} \frac{1}{\sqrt{\cos(\omega t) + iB \sin(\omega t)}}. \quad (24c)$$

Note that, for $B = 1$, (23) reduces to the usual ground state wave function of the harmonic oscillator. This suggests that the parameter B must be associated with the system's energy. To show this, we calculate the expected value of the Hamiltonian (20) on the state (23). The result is

$$\langle \hat{H} \rangle = \frac{(1 + B^2)\omega}{4B}. \quad (25)$$

From (25), it is clear that the minimum energy corresponds to $B = 1$, which is precisely the energy of the ground state.

On the other hand, since B is a continuous parameter, for $B \neq 1$, the state (23) corresponds to a linear combination of energy basis states. To show this, we begin by writing (14) in terms of this basis, which results in

$$\begin{aligned} \Psi(q, t; \lambda) &= \sum_{n=0}^{\infty} \exp(-iE_n t) u_n(q) \langle n | \Psi(0; \lambda) \rangle \\ &= \sum_{n=0}^{\infty} \frac{1}{\sqrt{(2n)! \mu \gamma}} \exp(-iE_{2n} t) u_{2n}(q) C(0; \lambda) 2^{n-1/2} \Gamma(n + 1/2) \left(1 - \frac{2}{\mu}\right)^n, \end{aligned} \quad (26)$$

where E_n are the energy eigenvalues of the system, $u_n(q) = \langle q | n \rangle$ and

$$\mu = 1 + \frac{U(0; \lambda) + iV(0; \lambda)}{\gamma^2} \quad (27)$$

with $\gamma = \sqrt{\omega/W}$. Substituting (24) in (26) and taking $u_n(q) = a_n \exp\left(-\frac{\gamma^2 q^2}{2}\right) H_n(\gamma q)$ we obtain for the Harmonic oscillator

$$\psi_{HO}(q, t; \lambda) = \frac{B^{1/4}}{\sqrt{1+B}} \sum_{n=0}^{\infty} \frac{e^{-iE_{2n} t} \sqrt{(2n)!}}{2^{n+1/2} n!} \left(\frac{1-B}{B+1}\right)^n u_{2n}(q), \quad (28)$$

which is the expansion of (23) in terms of energy basis states. From this expression, we can see that $\psi_{HO}(q, t; \lambda)$ is the ground state for $B = 1$, while for all other values of B , it is a linear combination of the even energy eigenstates.

We can also notice that for a given value of the average energy $\langle \hat{H} \rangle = \bar{E}$, Eq. (25) has two solutions for the parameter B , which are given by

$$B^\pm = \frac{2\bar{E} \pm \sqrt{4\bar{E}^2 - \omega^2}}{\omega}. \quad (29)$$

Notice that $B^+ > 1$, $B^- < 1$, and $B^+ B^- = 1$. Also, for the ground state, $B^+ = B^- = 1$.

We now take $\Lambda = \{\Lambda^I\} = (t, X, W, B)$ with $I = 0, 1, 2, 3$ as the varying parameters in the wave function (23) and proceed to compute the tQGT.

Using (24) together with (16), we obtain the components of the tQMT

$$g_{00} = \frac{(B^2 - 1)^2 \omega^2}{8B^2}, \quad (30a)$$

$$g_{01} = -\frac{(B^2 - 1)W((B^2 + 1)\sin(2\omega t) - 2(B^2 - 1)\omega t)}{32B^2\omega}, \quad (30b)$$

$$g_{02} = \frac{(B^2 - 1)X(2(B^2 - 1)\omega t + (B^2 + 1)\sin(2\omega t))}{32B^2\omega}, \quad (30c)$$

$$g_{03} = 0, \quad (30d)$$

$$g_{11} = \frac{-8(B^4 - 1)\omega t \sin(2\omega t) + B^4 + 8(B^2 - 1)^2(\omega t)^2 - (B^2 - 1)^2 \cos(4\omega t) + 6B^2 + 1}{256B^2X^2}, \quad (30e)$$

$$g_{12} = -\frac{B^4 - 8(B^2 - 1)^2(\omega t)^2 - (B^2 - 1)^2 \cos(4\omega t) + 6B^2 + 1}{256B^2\omega^2}, \quad (30f)$$

$$g_{22} = \frac{8(B^4 - 1)\omega t \sin(2\omega t) + B^4 + 8(B^2 - 1)^2(\omega t)^2 - (B^2 - 1)^2 \cos(4\omega t) + 6B^2 + 1}{256B^2W^2}, \quad (30g)$$

$$g_{13} = \frac{\cos(2\omega t)}{16BX}, \quad (30h)$$

$$g_{23} = -\frac{\cos(2\omega t)}{16BW}, \quad (30i)$$

$$g_{33} = \frac{1}{8B^2}. \quad (30j)$$

Some remarks about these metric components. First, notice that for both values of the parameter B given by (29), the metric component (30a) reduces to the same energy dispersion $g_{00} = \frac{2\bar{E}^2}{\omega} - \frac{\omega}{2}$. Also, all metric components diverge when $B \rightarrow 0$, which corresponds to infinite average energy (25). Furthermore, for $B = 1$ all the components of the QMT are bounded, and the metric $\tilde{g}[X, W]$ reduces to

$$\tilde{g}[X, W]_{B=1} = \begin{pmatrix} \frac{1}{32X^2} & -\frac{1}{32XW} \\ -\frac{1}{32XW} & \frac{1}{32W^2} \end{pmatrix}, \quad (31)$$

which corresponds to the quantum metric tensor of the ground state of the harmonic oscillator [26]. Lastly, for an arbitrary B ($\neq 1$), the components of the QMT with time dependence (excepting g_{13} and g_{23}) are unbounded as $\omega t \rightarrow \infty$.

Now, we analyze the tQMT components' behavior, giving particular attention to large ωt . We can distinguish two different behaviors.

- (i) The components g_{00} and g_{12} attain a minimum at $B = 1$; while g_{11} and g_{22} have a minimum at $B = B_{H+}$ and $B = B_{H-}$, respectively, where

$$B_{H\pm} = \sqrt{\frac{2\omega t \pm \sin(2\omega t)}{2\omega t \mp \sin(2\omega t)}}; \quad (32)$$

and finally, g_{01} and g_{02} have a minimum at $B = \sqrt{B_{H+}}$ and $B = \sqrt{B_{H-}}$, respectively. Notice that $B_{H\pm} \rightarrow 1$ when $\omega t \rightarrow \infty$. In fact, equation (32) can be written as $B_{H\pm} = 1 \pm \Delta B_H$. Hence, 'the vicinity of $B = 1$ ' in this context means the interval $[1 - |\Delta B_H|, 1 + |\Delta B_H|]$, with $\Delta B_H \ll 1$. Neglecting second-order terms on ΔB_H , we find $\Delta B_H \approx \frac{\sin 2\omega t}{2\omega t}$. From this, it is clear that as ωt increases, $B_{H\pm}$ approaches to 1. Then, the components (30a)-(30g) have a minimum in the vicinity of $B = 1$, corresponding to the ground state. This shows that our tQMT distinguishes the ground state of the system. This behavior can be appreciated in Fig. 1a, where we take $X = W = 1$ and $t = 10$.

- (ii) The components g_{13} , g_{23} , and g_{33} have a monotonic decreasing behavior, as we can see in Fig. 1b.

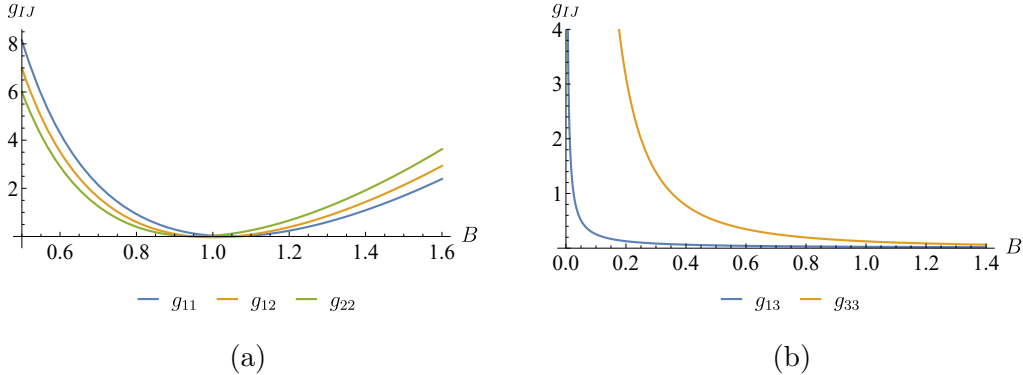


Figure 1: Some components of the tQMT, as a function of the parameter B . Except for g_{03} , the tQMT components are singular at $B = 0$. The remaining parameters were fixed as follows: $X = W = 1$ and $t = 10$. (a) These components have a minimum at around $B = 1$. (b) These components show a monotone behavior.

On the other hand, Fig. 2 shows the time evolution of the component g_{11} for three values of the parameter B . For $B = 1$, g_{11} is time-independent. This is because the metric reduces to that of the ground state for this value (see (31)). For $B = 1/2$ and

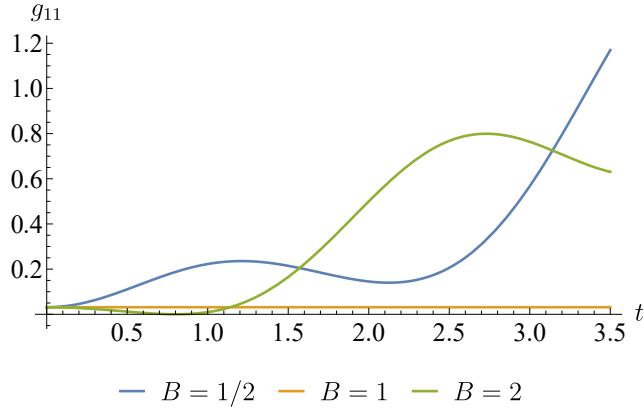


Figure 2: Component g_{11} of the tQMT in the region 1 as a function of time. The parameters were fixed as $X = W = 1$.

$B = 2$, g_{11} oscillates and increases, indicating that for variations of X the distance between the states increases.

It is remarkable that, in contrast to time-separable states, the wave function (23) leads to a tBerry curvature different from zero. Using (17) and (24), the components of this curvature are

$$F_{01} = \frac{(B^2 - 1) W \cos(2\omega t)}{8B\omega}, \quad (33a)$$

$$F_{02} = -\frac{(B^2 - 1) X \cos(2\omega t)}{8B\omega}, \quad (33b)$$

$$F_{03} = \frac{(B^2 - 1) \omega}{4B^2}, \quad (33c)$$

$$F_{12} = -\frac{(B^2 - 1) t \cos(2\omega t)}{8B\omega}, \quad (33d)$$

$$F_{23} = \frac{2(B^2 - 1)\omega t + (B^2 + 1)\sin(2\omega t)}{16B^2W}, \quad (33e)$$

$$F_{31} = \frac{(B^2 + 1)\sin(2\omega t) - 2(B^2 - 1)\omega t}{16B^2X}. \quad (33f)$$

In Fig. 3, we see that all the components of the curvature change sign in the vicinity of $B = 1$, which, according to (28), is the only value of B that corresponds to a stationary state. More precisely, F_{0i} and F_{12} , cross zero at $B = 1$, while F_{13} and F_{23} cross zero at $B = B_{H+}$ and $B = B_{H-}$, respectively.

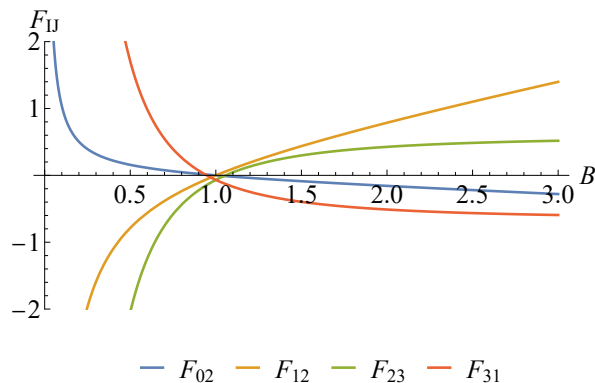


Figure 3: Non-zero components of the tBerry curvature in the region 1 by fixing $X = W = 1$. As a function of the parameter B , taking $t = 5$. They cross zero around $B = 1$.

On the other hand, in Fig. 4 we see that the tBerry curvature oscillates in time, which means that the probability distribution obtained from (23) oscillates between the two values of B that have the same energy, i.e., between 2 and $1/2$ in the case of Fig. 4.

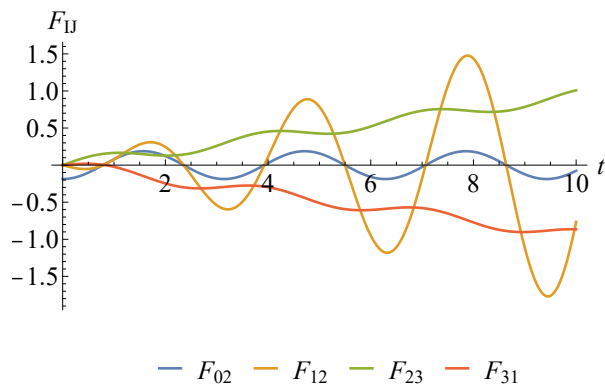


Figure 4: Non-zero components of the tBerry curvature for the harmonic oscillator as a function of time, taking $B = 2$.

3.1.1. Probability density We now analyze the behavior of the distribution probability $\rho_{HO}(q, t; B) = \psi_{HO}\psi_{HO}^*$, considering only the dependence on q , t , and B . We begin by noting that, as a function of time, $\rho_{HO}(q, t; B)$ has critical points ($\partial_t \rho_{HO} = 0$) at $t^* = \frac{n\pi}{2\omega}$ with $n \in \mathbb{Z}$. In particular, the second time derivative of ρ_{HO} evaluated at $q = 0$ and $t = t^*$ gives

$$\partial_t^2 \rho_{HO}(0, t_{\text{even}}^*; B) = -(B^2 - 1) \sqrt{\frac{B\omega^5}{W\pi}}, \quad (34a)$$

$$\partial_t^2 \rho_{HO}(0, t_{\text{odd}}^*; B) = \frac{B^2 - 1}{B^3} \sqrt{\frac{B\omega^5}{W\pi}}, \quad (34b)$$

where we have defined $t_{\text{even}}^* := \frac{n\pi}{\omega}$ and $t_{\text{odd}}^* := \frac{(2n+1)\pi}{2\omega}$. Due to the periodicity of ρ_{HO} , we can consider $t \in [0, \frac{2\pi}{\omega})$, then, the critical points reduces to $t_{\text{even}}^* = 0$ and $t_{\text{odd}}^* = \frac{\pi}{2\omega}$.

Notice that the second-time derivatives of ρ_{HO} given by (34) are positive or negative quantities depending on whether B is greater than or less than one. Furthermore, it is straightforward to see that for $B_{>}(B > 1)$ (respectively $B_{<}(B < 1)$) the critical points at t_{even}^* are maximums (respectively minimums), while the critical points at t_{odd}^* are minimums (respectively maximums). The values of ρ at the critical points are

$$\rho_{HO}(0, t_{\text{even}}^*; B) = \left(\frac{B\omega}{\pi^{1/2}W} \right)^{1/2}, \quad (35a)$$

$$\rho_{HO}(0, t_{\text{odd}}^*; B) = \left(\frac{\omega}{\pi^{1/2}BW} \right)^{1/2}. \quad (35b)$$

On the other hand, by the mean value theorem, there is a time $\tau \in (t_{\text{even}}^*, t_{\text{odd}}^*)$ such that $\rho_{HO}(0, \tau; B_{>}) = \rho_{HO}(0, \tau; B_{<})$. In particular, for $B_{<} = B_{>}^{-1}$, it can be shown that $\rho_{HO}(0, \tau; B_{>}) = \rho_{HO}(0, \tau; B_{>}^{-1})$ at $\tau = \frac{\pi(2n+1)}{4\omega}$. The previous analysis can be observed in Fig. 5, where we have set $X = W = 1$, and $B = 1/2, 2$.

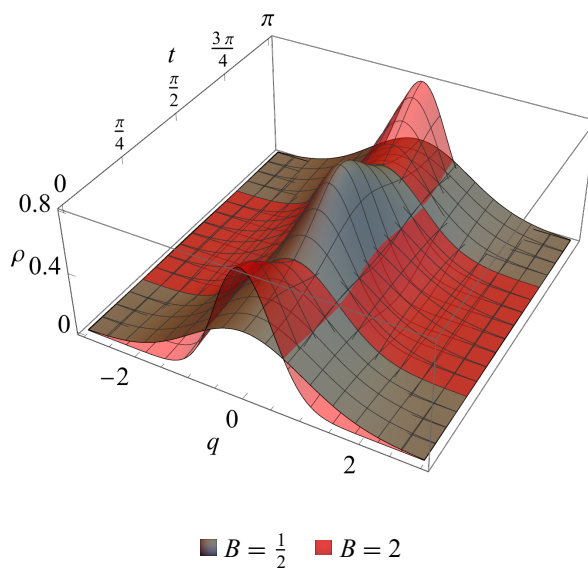


Figure 5: Distribution density probability as a function of q and t , with $X = W = 1$ and $B = 1/2, 2$. With this choice of parameters, $\rho(q, t; 1/2)$ and $\rho(q, t; 2)$ crosses at $\tau = \pi/4, 3\pi/4$

3.2. Region 2: inverted harmonic oscillator

The quantum dynamics of the inverted oscillator have been investigated for several years [22]. Over time, new characteristics of the system have been found, such as its relation to the zeros of the Riemann zeta function [27], or that it can be confined to give rise to a discrete spectrum [23], and more recently its application in understanding the quantum mechanics of dispersion and time decay in various systems [28]. Additionally, recent studies have shown that this system serves as an ideal toy model for understanding some ideas about chaos and complexity [29–31]. In this Section, we study the tQGT associated with the inverted oscillator by using a wave packet very similar to that described by Eq. (23) for the harmonic oscillator.

As we mentioned, we start by considering the initial state (21). In this case, the kernel of the inverted oscillator is

$$K(q', t; q, 0) = \sqrt{\frac{\alpha}{2\pi i W t}} \exp\left(-\frac{\alpha((q^2 + q'^2) \cosh(\alpha t) - 2qq')}{2iW \sinh(\alpha t)}\right), \quad (36)$$

where $\alpha = \sqrt{-XW}$, which is a real parameter function since $X < 0$ in this region. Using this kernel, the evolution over time of the initial condition (21) results in

$$\psi_{IHO}(q, t; \lambda) = \left(\frac{B\alpha}{W\pi}\right)^{1/4} \frac{1}{\sqrt{\cosh(\alpha t) + iB \sinh(\alpha t)}} \exp\left(-\frac{q^2}{2} \frac{\alpha(1 + iB \coth(\alpha t))}{W(-B + i \coth(\alpha t))}\right). \quad (37)$$

Comparing (37) and (14), we obtain the identifications

$$U_{IHO}(t, \lambda) = \frac{\alpha B \operatorname{csch}^2(\alpha t)}{W(B^2 + \coth^2(\alpha t))}, \quad (38a)$$

$$V_{IHO}(t, \lambda) = -\frac{\alpha(B^2 + 1) \coth(\alpha t)}{W(B^2 + \coth^2(\alpha t))}, \quad (38b)$$

$$C_{IHO}(t; \lambda) = \left(\frac{B\alpha}{W\pi}\right)^{1/4} \frac{1}{\sqrt{\cosh(\alpha t) + iB \sinh(\alpha t)}}. \quad (38c)$$

The expectation value of the Hamiltonian (20) on the state (37) turns out to be

$$\bar{E} = \langle \hat{H} \rangle = \frac{(-1 + B^2)\alpha}{4B}. \quad (39)$$

In this case, we also have two values of B that solve (39) for the same average of the Hamiltonian \bar{E} , namely

$$B_1 = \frac{2\bar{E} + \sqrt{\alpha^2 + 4\bar{E}^2}}{\alpha}, \quad B_2 = \frac{2\bar{E} - \sqrt{\alpha^2 + 4\bar{E}^2}}{\alpha}. \quad (40)$$

Notice that, only B_1 is physical, since B_2 is negative and then gives rise to a non-normalizable wave function.

Using the same varying parameters as before, $\Lambda = \{\Lambda^I\} = (t, X, W, B)$ with $I = 0, 1, 2, 3$, the components of the tQMT are given by

$$g_{00} = \frac{(B^2 + 1)^2 \alpha^2}{8B^2}, \quad (41a)$$

$$g_{01} = -\frac{(B^2 + 1)W(-(B^2 - 1)\sinh(2\alpha t) + 2(B^2 + 1)\alpha t)}{32B^2\alpha}, \quad (41b)$$

$$g_{02} = \frac{(B^2 + 1)X((B^2 - 1)\sinh(2\alpha t) + 2(B^2 + 1)\alpha t)}{32B^2\alpha}, \quad (41c)$$

$$g_{03} = 0, \quad (41d)$$

$$g_{11} = \frac{-8(B^4 - 1)\alpha t \sinh(2\alpha t) - B^4 + 8(B^2 + 1)^2(\alpha t)^2 + (B^2 + 1)^2 \cosh(4\alpha t) + 6B^2 - 1}{256B^2X^2}, \quad (41e)$$

$$g_{12} = -\frac{B^4 + 8(B^2 + 1)^2(\alpha t)^2 - (B^2 + 1)^2 \cosh(4\alpha t) - 6B^2 + 1}{256(B\alpha)^2}, \quad (41f)$$

$$g_{22} = \frac{8(B^4 - 1)\alpha t \sinh(2\alpha t) - B^4 + 8(B^2 + 1)^2(\alpha t)^2 + (B^2 + 1)^2 \cosh(4\alpha t) + 6B^2 - 1}{256B^2X^2}, \quad (41g)$$

$$g_{13} = \frac{\cosh(2\alpha t)}{16BX}, \quad (41h)$$

$$g_{23} = -\frac{\cosh(2\alpha t)}{16BW}, \quad (41i)$$

$$g_{33} = \frac{1}{8B^2}. \quad (41j)$$

From (41), we can see that some components exhibit a hyperbolic function-like time dependence, leading to an exponential asymptotic behavior as $\alpha t \rightarrow \infty$. We now analyze the behavior of these metric components, paying particular attention to the asymptotic limit as $\alpha t \rightarrow \infty$. Here, we can distinguish three different cases.

- (i) The components g_{01} and g_{02} lose their hyperbolic time dependence at $B = 1$. Furthermore, g_{01} and g_{02} vanish at B_{I+} and B_{I-} , respectively, with

$$B_{I\pm} = \sqrt{\frac{\sinh(2\alpha t) \pm 2\alpha t}{\sinh(2\alpha t) \mp 2\alpha t}}. \quad (42)$$

This means that g_{01} crosses zero at $B < 1$, while g_{02} crosses zero at $B > 1$. Notice that $B_{I\pm} \rightarrow 1$ when $\omega t \rightarrow \infty$. Now, we proceed similarly to the harmonic case, rewriting (42) as $B_{I\pm} = 1 \pm \Delta B_I$. Hence, ‘the neighbourhood of $B = 1$ ’ in this context means the interval $[1 - |\Delta B_I|, 1 + |\Delta B_I|]$, with $\Delta B_I \ll 1$. Neglecting second-order terms on ΔB_I , we find $\Delta B_I \approx \frac{2\alpha t}{\sinh 2\alpha t}$. Then, for large αt (i.e. αt such that $\frac{2\alpha t}{\sinh 2\alpha t} \ll 1$), the components g_{01} and g_{02} are equal to zero in the neighborhood of 1, which corresponds to the point where the average energy changes from positive to negative. This behavior can be appreciated in Fig. 6a, where we have set $X = -1$, $W = 1$, and $t = 3$. For this choice of parameters, we have $\Delta B \approx 0.0297$.

- (ii) The component g_{00} have a minimum at $B = 1$. Furthermore, g_{11} , g_{22} , and g_{12} have a minimum at B_{I+} , B_{I-} , and $B = 1$ respectively. Then, for the larger αt , the minimum of g_{11} and g_{22} is closer to $B = 1$. In particular, this minimum occurs at $B \rightarrow 1$ as $\alpha t \rightarrow \infty$. See Fig. 6b
- (iii) The components g_{13} , g_{23} , and g_{33} have a monotonic behavior. See Fig. 6c, where we have used $X = -1$, $W = 1$, and $t = 3$, for which $g_{13} = g_{23}$.

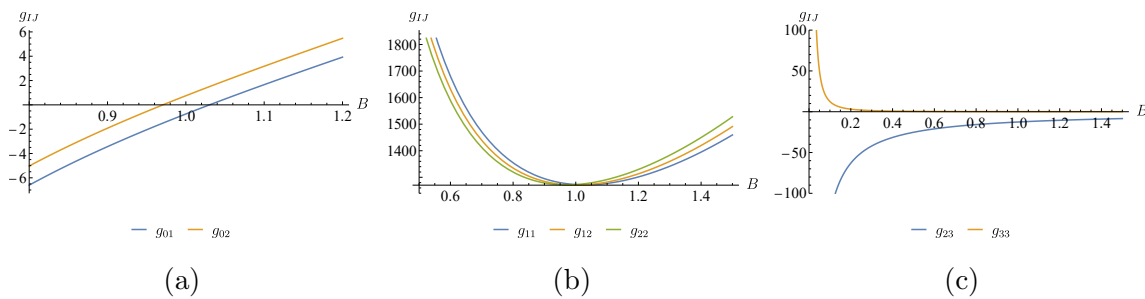


Figure 6: Components of the tQMT for the region 2, as a function of the parameter B , all of them are singular at $B = 0$. (a) Components g_{01} and g_{02} of the tQMT. g_{01} crosses zero at the right of $B = 1$, while g_{02} crosses zero at the left of $B = 1$. (b) These components have a minimum around $B = 1$. (c) These components show a monotone behavior.

In Fig. 7 we plot g_{11} as a function of t . Here we can see that this metric component exhibits an exponential behavior for large t . The other metric components with time dependence have a similar behavior.

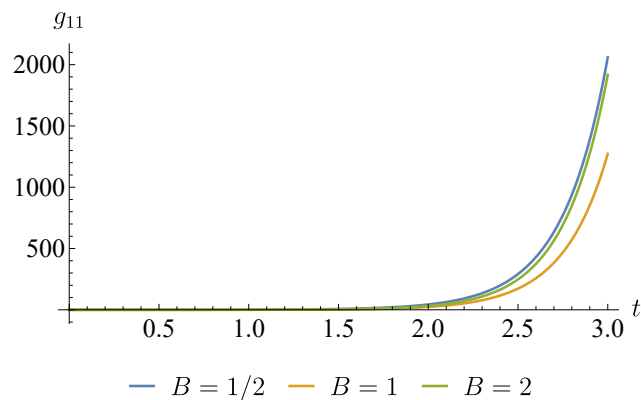


Figure 7: Component g_{11} of the tQMT in the region 2 as a function of time. The parameters were fixed as $X = -1$ and $W = 1$.

Now we will focus on tBerry curvature. The components of this tensor are

$$F_{01} = -\frac{(B^2 + 1) W \cosh(2at)}{8B\alpha}, \quad (43a)$$

$$F_{02} = \frac{(B^2 + 1) X \cosh(2at)}{8B\alpha}, \quad (43b)$$

$$F_{03} = \frac{(B^2 + 1) \alpha}{4B^2}, \quad (43c)$$

$$F_{12} = \frac{(B^2 + 1) t \cosh(2at)}{8B\alpha}, \quad (43d)$$

$$F_{13} = \frac{2(B^2 + 1) t\alpha - (B^2 - 1) \sinh(2at)}{16B^2 X}, \quad (43e)$$

$$F_{23} = \frac{2(B^2 + 1) t\alpha + (B^2 - 1) \sinh(2at)}{16B^2 W}. \quad (43f)$$

Let us first examine the behavior of these components as a function of B . Notice that at $B = 1$ the components F_{01} and F_{02} exhibit a minimum, while the component F_{12} has a maximum. Furthermore, the components F_{13} and F_{23} are zero at $B = B_+$ and $B = B_-$, respectively. The behavior of these components as a function of B is illustrated in Fig. 8. On the other hand, excepting F_{03} , all the components show a hyperbolic behavior as a function of t (see Fig. 9).

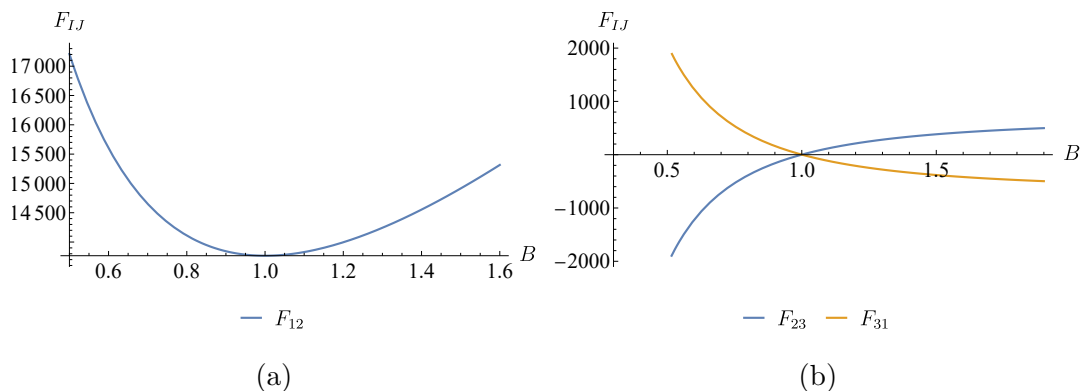


Figure 8: Components of the tBerry curvature for the region 2, as functions of the parameter B . The remaining parameters are fixed as follows: $X = -1$, $W = 1$, and $t = 5$. (a) This component has a minimum at $B = 1$, F_{01} and F_{02} have a similar behavior. (b) These components show a monotone-decreasing behavior.

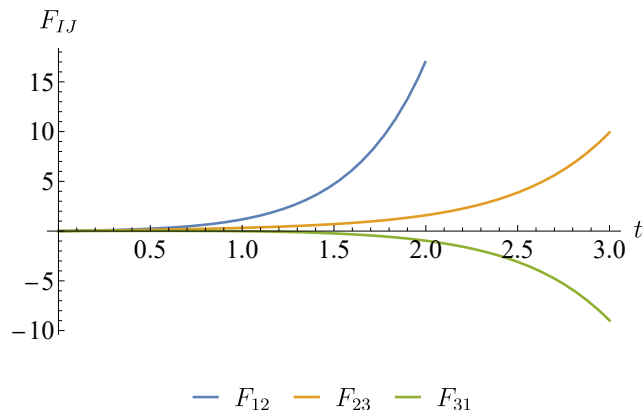


Figure 9: Components of the tBerry curvature in the region 2 as a function of time. The parameters were fixed as $W = B = 1$ and $X = -1$.

3.3. Transition zone

The goal now is to analyze the behavior of the tQMT near the bifurcation point at $X = 0$, where the system transitions from a harmonic to an inverted oscillator. The key features of the tQMT at the vicinity of $X = 0$ are:

- (i) The parameter component g_{ij} in region 1 has the same asymptotic behavior of the corresponding g_{ij} in region 2, at $X \rightarrow 0$.

- (ii) In both regions, the components g_{11} , g_{12} and g_{13} diverge at $X \rightarrow 0$, their asymptotic behavior at this point is $g_{11} \sim \frac{1}{32X^2}$, $g_{12} \sim -\frac{1}{32XW}$ and $g_{13} \sim \frac{1}{16XB}$. In Fig. 10a we plot g_{11} , showing its behavior at $X \rightarrow 0$.
- (iii) The components g_{00} , g_{01} , and g_{02} are continuous but not differentiable at $X = 0$.

Regarding the tBerry curvature, we observe a behavior analogous to that of the tQMT in the vicinity of $X = 0$. At $X \rightarrow 0$, the components F_{12} and F_{13} are singular (see Fig. 10b), while the remaining non-zero components are continuous but not differentiable.

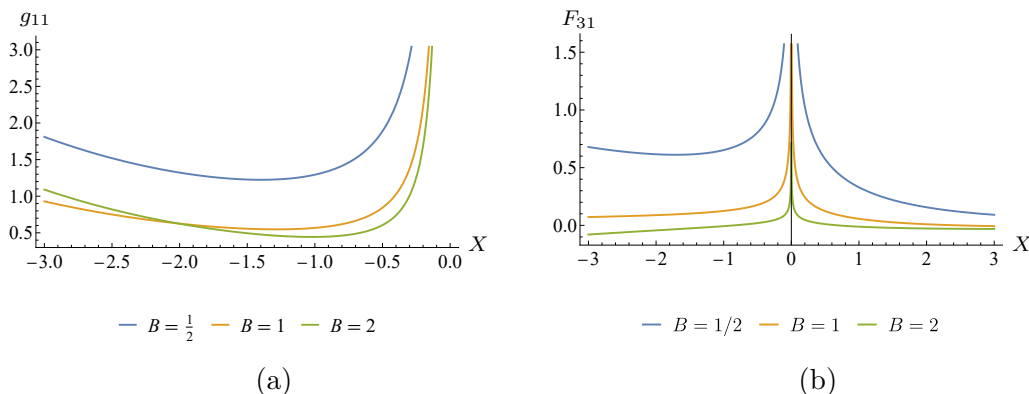


Figure 10: (a) Component g_{11} of the tQMT, and (b) component F_{31} of the tBerry curvature with $t = 1$. Both g_{11} and F_{31} are singular $X \rightarrow 0$, corresponding to the bifurcation point from the harmonic oscillator to the inverted oscillator.

The analysis clearly shows that the metric components g_{1i} and tBerry curvature components F_{1I} diverge at $X \rightarrow 0$, representing the point at which the system shifts from a Harmonic oscillator to an inverted one.

4. Harmonic oscillator with time-dependent frequency

In this section, we study a system whose Hamiltonian explicitly depends on time. We consider the harmonic oscillator with time-dependent frequency (HOTDF), whose Hamiltonian is given by

$$\hat{H}(\hat{q}, \hat{p}, \Lambda) = \frac{\hat{p}^2}{2} + \omega(\Lambda)^2 \frac{\hat{q}^2}{2}, \quad (44)$$

where $\Lambda = \{\Lambda^I\}$ ($I, J, \dots = 0, 1, \dots, \mathcal{N}$) is the set of time and parameters. In general, methods to solve problems with explicit time dependence are an open subject nowadays. An approach for solving these types of problems is to find constants of motion or invariants.

For the HOTDF there exists an invariant operator \hat{L} , known as the Lewis invariant, which is given by

$$\hat{L} = \frac{1}{2} \left(\frac{\hat{q}^2}{\gamma^2} + (\gamma\hat{p} - \hat{q}\dot{\gamma})^2 \right), \quad (45)$$

where γ satisfies the Ermakov equation

$$\frac{d^2\gamma}{dt^2} + \omega^2(\Lambda)\gamma - \frac{1}{\gamma^3} = 0. \quad (46)$$

The existence of this invariant operator is of utmost importance in solving the corresponding time-dependent Schrodinger equation. Lewis and Riesenfeld [32,33] have shown that the general solution is given by the superposition

$$|\Psi(\Lambda)\rangle = \sum_n c_n e^{i\beta_n(t)} |n_L(\Lambda)\rangle, \quad (47)$$

where $|n_L(\Lambda)\rangle$ are the normalized eigenkets of the Lewis operator, i.e.,

$$\hat{L}|n_L(\Lambda)\rangle = \left(n + \frac{1}{2}\right) |n_L(\Lambda)\rangle, \quad (48)$$

and $\beta_n(t)$ are time-dependent phases, obtained from the equation

$$\frac{d\beta_n}{dt} = \dot{\beta}_n = \langle n_L(\Lambda) | i\partial_t - \hat{H} | n_L(\Lambda) \rangle. \quad (49)$$

The solutions to equations (48) and (49) are, respectively, given by

$$\psi_{n_L}(q; \Lambda) = \langle q | n_L(\Lambda) \rangle = \frac{\exp\left(-\left(\frac{1}{\gamma^2} - i\frac{\dot{\gamma}}{\gamma}\right)\frac{q^2}{2}\right)}{\sqrt{2^n n! |\gamma| \sqrt{\pi}}} H_n\left(\frac{q}{|\gamma|}\right), \quad (50a)$$

$$\beta_n(t) = -\left(n + \frac{1}{2}\right) h(t), \quad (50b)$$

with h obtained through the equation $\dot{h} = \frac{1}{\gamma^2}$. To simplify our calculations, we consider the case where all the coefficients c_n involved in (47), except one, are zero. Hence, under this consideration (47) reduces to

$$|\Psi(\Lambda)\rangle = e^{i\beta_n(t)} |n_L(\Lambda)\rangle. \quad (51)$$

We now proceed to compute the tQMT associated with the quantum state (51). Analogously to what happens in the case of a stationary state, the tQMT turns out to be independent of the time-dependent phase $\beta_n(t)$. In fact, substituting (51) into (5) we get

$$Q_{IJ}(\Lambda) = \langle \partial_I n_L | \partial_J n_L \rangle - \langle \partial_I n_L | n_L \rangle \langle n_L | \partial_J n_L \rangle. \quad (52)$$

However, in contrast to the stationary state case (see (13)), (52) is time-dependent since $|n_L(\Lambda)\rangle$ is.

Using the eigenfunction (50a), and taking the real and imaginary part of (52), we find that the components of the tQMT and the tBerry curvature are

$$g_{IJ} = \frac{\gamma^4(n^2 + n + 1)}{8} \left(\partial_I \left(\frac{\dot{\gamma}}{\gamma}\right) \partial_J \left(\frac{\dot{\gamma}}{\gamma}\right) + (\partial_I \gamma^{-2}) (\partial_J \gamma^{-2}) \right), \quad (53a)$$

$$F_{IJ} = \frac{\gamma^4(2n + 1)}{4} \left((\partial_J \gamma^{-2}) \partial_I \left(\frac{\dot{\gamma}}{\gamma}\right) - (\partial_I \gamma^{-2}) \partial_J \left(\frac{\dot{\gamma}}{\gamma}\right) \right), \quad (53b)$$

respectively.

This system exhibits some properties analogous to those of the model described by the wavefunction (14). In particular, it can be verified that the metric (53a) satisfies the relations (19a) and (19c). Nevertheless, instead of (19b), the relation between (53a) and (53b) is given by

$$\det \tilde{\mathbf{g}}[\Lambda^{I_1}, \Lambda^{I_2}] = \frac{(2n+1)^2}{4(n^2+n+1)^2} (F_{I_1 I_2})^2, \quad \text{if } \mathcal{N} = 2, \quad (54)$$

which coincides with (19b) for $n = 0$.

Let us now consider a specific example in which the frequency is given by

$$\omega(t) = \sqrt{\omega_0^2 e^{2At} - \frac{A^2}{4}}, \quad (55)$$

where $\omega_0^2 e^{2At} - \frac{A^2}{4} > 0$. Then, the set of time and system parameters is $\Lambda = \{\Lambda^I\} = \{t, A, \omega_0\}$, with $I = 0, 1, 2$. Notice if $A = 0$, the frequency becomes constant, recovering the usual harmonic oscillator with squared frequency ω_0^2 . For the frequency (55) we obtain the explicit solution for γ and h , obtaining $\gamma = e^{-At/2}$ and $h = \omega_0 e^{At}/A$. Substituting these expressions into (53a) and (53b), we find that the metric is

$$g_{IJ} = \frac{n^2 + n + 1}{8} \begin{pmatrix} A^2 & At & \frac{A}{\omega_0} \\ At & \frac{e^{-2At}}{4\omega_0^2} + t^2 & \frac{t}{\omega_0} \\ \frac{A}{\omega_0} & \frac{t}{\omega_0} & \frac{1}{\omega_0^2} \end{pmatrix}, \quad (56)$$

and that the tBerry curvature is

$$F_{IJ} = \frac{(2n+1)e^{-At}}{8\omega_0^2} \begin{pmatrix} 0 & A\omega_0 & 0 \\ -A\omega_0 & 0 & -1 \\ 0 & 1 & 0 \end{pmatrix}. \quad (57)$$

Notice that the component g_{00} is time-independent, implying that the energy dispersion remains constant in this case. Also, components g_{0I} and F_{0I} vanish if $A = 0$, in which case our state becomes a stationary state. Furthermore, for $t \rightarrow \infty$ the tBerry (57) tends to 0, corresponding to a zero phase interference in this limit.

Notice that the system corresponds to a free particle in the limit $\omega(t) = 0$. There are two cases where frequency (55) vanishes: a) both parameters A and ω_0 tend to zero and b) $4\omega_0^2 - A^2 e^{-2At}$ tends to zero. Both cases are reflected in the metric and tBerry curvature. For case a) we have that the metric components g_{00} and g_{01} tend zero and the rest become undefined. For the curvature, all its components become undefined. Then, as expected, we have a breakdown of the geometric structure in this limit because the system would correspond to a free particle and not to an oscillator anymore. On the other hand, for b) we have the curvature component F_{01} becomes constant, i.e., independent of the parameters. This is reflected in the metric, because of the Palumbo-Goldman relation (54), as $\det \tilde{\mathbf{g}}[t, A] \rightarrow \frac{n^2+n+1}{8}$.

5. Coupled systems

In this Section, we consider a system of N coupled particles described by a wave function corresponding to a generalization of (14) and analyze the associated tQMT and tBerry curvature. In normal coordinates $Q = \{Q_a\}$ with $a = 1, \dots, N$, the generalized wave function is given by

$$\psi(Q, \Lambda) = C(\Lambda) \exp\left(-\sum_{a=1}^N (U^a(\Lambda) + iV^a(\Lambda)) Q_a^2/2\right), \quad (58)$$

where $U^a(\Lambda) > 0$, $V^a(\Lambda) \in \mathbb{R}$, $C(\Lambda) \in \mathbb{C}$, and $\Lambda = \{\Lambda^I\}$ ($I, J, \dots = 0, 1, \dots, \mathcal{N}$) is the set of time and parameters. The normalization condition of the wave function implies

$$|C(\Lambda)|^2 = \pi^{-N/2} \prod_{a=1}^N \sqrt{U^a(\Lambda)}. \quad (59)$$

Using (4) and (58), it is found that the components of the tQMT are given by

$$g_{IJ} = \sum_{a=1}^N \frac{\partial_I U^a \partial_J U^a + \partial_I V^a \partial_J V^a}{8(U^a)^2}. \quad (60)$$

Notice that the tQMT has dimensions of $(\mathcal{N} + 1) \times (\mathcal{N} + 1)$. On the other hand, if we consider that all functions U^a and V^b are distinct from each other and that there is no functional dependency between them (i.e., $U^b \neq f(U^1, \dots, U^{b-1}, U^{b+1}, \dots, U^N, V)$ and $V^b \neq f(U, V^1, \dots, V^{b-1}, V^{b+1}, \dots, V^N)$), then the metric is generated by a set of $2N$ independent functions $\{U^a, V^a\}$. Here $U = \{U^a\}$ and $V = \{V^a\}$. It can be shown by induction on N that the determinant of the metric is zero if $\mathcal{N} = 2N$.

Now, let us consider the case where there is functional dependency among the functions U and V with multiplicity l . Then, we can define a constraint surface given by l functions that relate the functions U^a and V^a among themselves, this can be written as

$$\begin{aligned} f_1(U, V) &= 0, \\ &\vdots \\ f_l(U, V) &= 0. \end{aligned} \quad (61)$$

In this scenario, the determinant of the metric (60) is zero if $\mathcal{N} > 2N - l - 1$, which means that there can be at most $2N - l$ independent parameters. Taking this into account, in the following, we consider metrics $\tilde{\mathbf{g}}[\Lambda^{I_1}, \dots, \Lambda^{I_\eta}]$ obtained from the variation of η elements $\Lambda^{I_1}, \dots, \Lambda^{I_\eta}$ (with $I_1, \dots, I_\eta \in 0, \dots, \mathcal{N}$).

For a more comprehensive analysis, it would be of interest to calculate the scalar curvature $\mathcal{R}[\Lambda^{I_1}, \dots, \Lambda^{I_\eta}]$ associated with the metrics $\tilde{\mathbf{g}}[\Lambda^{I_1}, \dots, \Lambda^{I_\eta}]$. Nevertheless, the calculations for the scalar curvature are quite involved when the functions U^a and V^a are arbitrary, and hence, we restrict ourselves to the case $N = 2$, where the maximum

number of independent parameters is $\eta = 4$. In addition, the resulting expressions for the Ricci tensor for $\eta = 2, 3$, when keeping U^a and V^a arbitrary, are too lengthy and do not yield substantial information. In the case $N = 2$ and $\eta = 4$, for arbitrary functions U^a and V^a , the scalar curvature takes the remarkable simple form

$$\mathcal{R}[\Lambda^{I_1}, \dots, \Lambda^{I_4}] = -32. \quad (62)$$

This expression and (19c), which corresponds to the case where $N = 1$ and $\eta = 2$, suggest the possibility of obtaining an analogous expression for the scalar curvature $\mathcal{R}[\Lambda^{I_1}, \dots, \Lambda^{I_{2N}}]$ in the case $N > 2$ and $\eta = 2N$. However, the calculations for $N > 2$, using arbitrary functions U^a and V^a , result in extensive procedures. Particularly, for several specific examples and $N = 3, 4, 5, 6$, we find that the scalar curvature is given by

$$\mathcal{R}[\Lambda^{I_1}, \dots, \Lambda^{I_{2N}}] = -16N. \quad (63)$$

Although this is not a formal proof, it suggests the hypothesis that this property holds for all N and any set of functionally independent functions U^a and V^a .

On the other hand, using (6) and (58), we find that the components of the tBerry curvature are

$$F_{IJ} = \sum_{a=1}^N \frac{-\partial_I U^a \partial_J V^a + \partial_I V^a \partial_J U^a}{4(U^a)^2}. \quad (64)$$

The previous cases will now be analyzed in detail for a chain of generalized oscillators, where the functions U^a and V^a are known. Specifically, a system that admits solutions of the form (58) is a generalization of the system of one particle described by Hamiltonian (20) to a system of N particles described by the Hamiltonian

$$\hat{H}(\hat{q}, \hat{p}, \Lambda) = \frac{1}{2} \hat{p}^\top \hat{p} + \frac{1}{2} \hat{q}^\top \mathbf{K} \hat{q} + \frac{Y}{2} (\hat{q}^\top \hat{p} + \hat{p}^\top \hat{q}), \quad (65)$$

where $\hat{q} = (\hat{q}_1, \dots, \hat{q}_N)^\top$, $\hat{p} = (\hat{p}_1, \dots, \hat{p}_N)^\top$, and

$$\mathbf{K} = Z\mathbf{A} + X\mathbf{1}, \quad (66)$$

with \mathbf{A} a $N \times N$ matrix of constant coefficients and $\mathbf{1}$ the $N \times N$ identity matrix. It is worth noting that the Hamiltonian (65) involves the term with Y , which is not present in Hamiltonian (20). Because of this, in one dimension, this system is referred to as the generalized harmonic oscillator and it is well-known to exhibit non-trivial Berry curvature [34].

Through the canonical transformation $\hat{q} = \mathbf{S}\hat{Q}$ and $\hat{p} = \mathbf{S}(\hat{P} - Y\hat{Q})$, the Hamiltonian (65) can be expressed as

$$\hat{H}(\hat{Q}, \hat{P}, \Lambda) = \frac{1}{2} \hat{P}^\top \hat{P} + \frac{1}{2} \hat{Q}^\top \mathbf{\Omega}^2 \hat{Q}. \quad (67)$$

Here, the matrix \mathbf{S} diagonalizes $\mathbf{M} = \mathbf{K} - Y^2 \mathbf{1}$, and $\mathbf{\Omega} = \text{diag}(\omega_1, \dots, \omega_N)$, where ω_a^2 , with $a = 1, \dots, N$, represents the eigenvalues of \mathbf{M} ; that is, $\mathbf{S}^\top \mathbf{M} \mathbf{S} = \mathbf{\Omega}^2$. The normal frequencies ω_b are given by

$$\omega_b = \sqrt{a_b Z + X - Y^2}, \quad (68)$$

where a_b are the eigenvalues of \mathbf{A} .

We assume that $\omega_{c+1}^2 > \omega_c^2$ for $c = 1, \dots, N-1$. This condition requires that all eigenvalues of \mathbf{A} be distinct. Analogous to the case $N = 1$, where we have considered two regions, in the general N -dimensional system we can consider $N+1$ regions, depending on the value of the parameters. The m -th region, with $m = 1, \dots, N+1$, corresponds to the first $m-1$ normal modes behaving as inverted harmonic oscillators, while the remaining $N-m+1$ modes are harmonic oscillators. For $a_b Z + X - Y^2 < 0$, we introduce the real parameter functions $\alpha_b = \sqrt{Y^2 - a_b Z - X}$ ($b = 1, \dots, N$). In this scenario, it is convenient to rewrite the Hamiltonian for the m -th region with $m = 2, \dots, N$ as

$$H_m(\hat{Q}, \hat{P}, \Lambda) = \frac{1}{2} \sum_{c=1}^{m-1} (\hat{P}_c^2 - \alpha_c^2 \hat{Q}_c^2) + \frac{1}{2} \sum_{d=m}^N (\hat{P}_d^2 + \omega_d^2 \hat{Q}_d^2), \quad (69)$$

where we have introduced the sub-index m to point out that we are in the m -th region (alternative, that we have $m-1$ normal modes that behave as inverted oscillators, which we call *inverted normal modes*). In the case $m = 1$ there are only harmonic normal modes, whereas in the case $m = N+1$ there are exclusively inverted normal modes.

As in the previous Section, we consider solutions of the time-dependent Schrödinger equation for the Hamiltonian (69) that are non-time-separable. More precisely, we consider solutions of the form

$$\Psi_m(Q, \Lambda) = \prod_{d=1}^{m-1} \chi_d(Q_d, \Lambda) \prod_{c=m}^N \psi_c(Q_c, \Lambda), \quad (70)$$

where

$$\chi_d(Q_d, \Lambda) = \left(\frac{B_d \alpha_d}{\pi} \right)^{1/4} \frac{\exp \left(-\frac{Q_d^2 \alpha_d}{2} \frac{(1+iB_d \coth(t\alpha_d))}{(-B_d+i \coth(\alpha_d t))} - \frac{iY Q_d^2}{2} \right)}{\sqrt{\cosh(\alpha_d t) + iB_d \sinh(\alpha_d t)}}, \quad (71)$$

is a solution for an inverted normal mode and

$$\psi_c(Q_c, \Lambda) = \left(\frac{B_c \omega_c}{\pi} \right)^{1/4} \frac{\exp \left(-\frac{Q_c^2 \omega_c}{2} \frac{(1-iB_c \cot(\omega_c t))}{(B_c-i \cot(\omega_c t))} - \frac{iY Q_c^2}{2} \right)}{\sqrt{\cos(\omega_c t) + iB_c \sin(\omega_c t)}}, \quad (72)$$

is a solution for a Harmonic one.

In particular, for the cases $m = 1$ and $m = N+1$, we have

$$\Psi_1(Q, \Lambda) = \prod_{c=1}^N \psi_c(Q_c, \Lambda), \quad (73a)$$

$$\Psi_{N+1}(Q, \Lambda) = \prod_{d=1}^N \chi_d(Q_d, \Lambda), \quad (73b)$$

respectively. Notice that in these wave functions the parameters are $\Lambda = \{\Lambda^0, \Lambda^i\} = \{t, X, Y, Z, B_1, \dots, B_N\}$ with $i = 1, 2, \dots, N + 3$. Note also that the solution (70) can be written as (58), by making the following identifications:

$$U_m^a(\Lambda) = \begin{cases} U_\psi^a(\Lambda) & \text{if } a \geq m, \\ U_x^a(\Lambda) & \text{if } a < m, \end{cases} \quad (74a)$$

$$V_m^a(\Lambda) = \begin{cases} V_\psi^a(\Lambda) & \text{if } a \geq m, \\ V_x^a(\Lambda) & \text{if } a < m, \end{cases} \quad (74b)$$

$$C_m(\Lambda) = \prod_{a=m}^N C_\psi^a(\Lambda) \prod_{a=1}^{m-1} C_x^a(\Lambda), \quad (74c)$$

where

$$U_\psi^a(\Lambda) = \frac{B_a \omega_a \csc^2(\omega_a t)}{B_a^2 + \cot^2(\omega_a t)}, \quad (75a)$$

$$V_\psi^a(\Lambda) = Y - \frac{(B_a^2 - 1) \omega_a \cot(\omega_a t)}{B_a^2 + \cot^2(\omega_a t)}, \quad (75b)$$

$$C_\psi^a(\Lambda) = \left(\frac{B_a \omega}{\pi} \right)^{1/4} \frac{1}{\sqrt{\cos(\omega_a t) + i B_a \sin(\omega_a t)}}, \quad (75c)$$

$$U_x^a(\Lambda) = \frac{B_a \alpha_a \operatorname{csch}^2(\alpha_a t)}{B_a^2 + \operatorname{coth}^2(\alpha_a t)}, \quad (75d)$$

$$V_x^a(\Lambda) = Y - \frac{(B_a^2 + 1) \alpha_a \operatorname{coth}(\alpha_a t)}{B_a^2 + \operatorname{coth}^2(\alpha_a t)}, \quad (75e)$$

$$C_x^a(\Lambda) = \left(\frac{B_a \alpha}{\pi} \right)^{1/4} \frac{1}{\sqrt{\cosh(\alpha_a t) + i B_a \sinh(\alpha_a t)}}. \quad (75f)$$

For the regions $m = 1$, $m = 2, \dots, N$, and $m = N + 1$ the expectation value of the Hamiltonian is respectively given by

$$\langle \hat{H}_1 \rangle = \sum_{d=1}^N \frac{(1 + B_d^2) \omega_d}{4B_d}, \quad (76a)$$

$$\langle \hat{H}_m \rangle = \sum_{c=1}^{m-1} \frac{(-1 + B_c^2) \alpha_c}{4B_c} + \sum_{d=m}^N \frac{(1 + B_d^2) \omega_d}{4B_d}, \quad (76b)$$

$$\langle \hat{H}_{N+1} \rangle = \sum_{c=1}^N \frac{(-1 + B_c^2) \alpha_c}{4B_c}. \quad (76c)$$

5.1. Particular case

For the purpose of providing a specific example, let us consider $N = 2$ and

$$\mathbf{A} = \begin{pmatrix} 2 & -1 \\ -1 & 2 \end{pmatrix},$$

which has eigenvalues $a_1 = 1$ and $a_2 = 3$. In this case, the Hamiltonian (65) reduces to

$$\hat{H} = \frac{1}{2} (\hat{p}_1^2 + \hat{p}_2^2 + Y (\hat{q}_1 \hat{p}_1 + \hat{p}_1 \hat{q}_1 + \hat{q}_2 \hat{p}_2 + \hat{p}_2 \hat{q}_2)) + \frac{1}{2} (X + 2Z) (\hat{q}_1^2 + \hat{q}_2^2) - Z \hat{q}_1 \hat{q}_2. \quad (77)$$

As we have explained, depending on the value of the subset of the parameters $\{Y, X, Z\}$, we can consider three regions (once it is written in the normal modes):

- Region 1: ω_1 and ω_2 are real.
- Region 2: α_1 and ω_2 are real.
- Region 3: α_1 and α_2 are real.

Notice that there is no region such that ω_1 and α_2 are real. This is because, as mentioned previously, the squared normal frequencies are ordered increasingly. Accordingly, the Hamiltonians, in normal coordinates, for each of these regions are

$$\hat{H}_1 = \frac{1}{2} (\hat{P}_1^2 + \omega_1^2 \hat{Q}_1^2) + \frac{1}{2} (\hat{P}_2^2 + \omega_2^2 \hat{Q}_2^2), \quad (78a)$$

$$\hat{H}_2 = \frac{1}{2} (\hat{P}_1^2 - \alpha_1^2 \hat{Q}_1^2) + \frac{1}{2} (\hat{P}_2^2 + \omega_2^2 \hat{Q}_2^2), \quad (78b)$$

$$\hat{H}_3 = \frac{1}{2} (\hat{P}_1^2 - \alpha_1^2 \hat{Q}_1^2) + \frac{1}{2} (\hat{P}_2^2 - \alpha_2^2 \hat{Q}_2^2). \quad (78c)$$

Furthermore, using (70), (73a) and (73b), we get the solutions of the corresponding Schrödinger equations

$$\Psi_1(Q, \Lambda) = \psi_1(Q_1, \Lambda) \psi_2(Q_2, \Lambda), \quad (79a)$$

$$\Psi_2(Q, \Lambda) = \chi_1(Q_1, \Lambda) \psi_2(Q_2, \Lambda), \quad (79b)$$

$$\Psi_3(Q, \Lambda) = \chi_1(Q_1, \Lambda) \chi_2(Q_2, \Lambda), \quad (79c)$$

and the expectation values

$$\langle \hat{H}_1 \rangle = \frac{(1 + B_1^2) \omega_1}{4B_1} + \frac{(1 + B_2^2) \omega_2}{4B_2}, \quad (80a)$$

$$\langle \hat{H}_2 \rangle = \frac{(-1 + B_1^2) \alpha_1}{4B_1} + \frac{(1 + B_2^2) \omega_2}{4B_2}, \quad (80b)$$

$$\langle \hat{H}_3 \rangle = \frac{(-1 + B_1^2) \alpha_1}{4B_1} + \frac{(-1 + B_2^2) \alpha_2}{4B_2}. \quad (80c)$$

Following the approach introduced in Section 2, we calculate the tQMT and tBerry curvature for the three regions, and taking $\{\Lambda^I\} = \{t, X, Y, Z, B_1, B_2\}$ with $I = 0, 1, \dots, 5$. We then examine whether there is any smoothness in these quantities as we move from one region to another. Some remarks for each region, in order, are as follows:

- (i) In region 1, only trigonometric functions are present in the tQMT and tBerry curvature. In the case $B_1 = B_2 = 1$, the components g_{nl} with $(n, l = 1, 2, 3)$ become time-independent. Also, the components g_{0I} becomes zero at $B_1 = B_2 = 1$

- (ii) In region 2, both trigonometric and hyperbolic functions appear in the tQMT and tBerry curvature.
- (iii) In region 3, only hyperbolic functions emerge in the tQMT and tBerry curvature.

Notably, the components g_{00} , g_{44} , g_{45} , and g_{55} are time-independent and g_{04} , g_{05} , and F_{13} are zero, across all regions. Also, g_{04} and g_{05} vanish in agreement with the one degree of freedom case, where $g_{03} = 0$. Generally, the resulting expressions for tQMT and tBerry curvature are too large to be explicitly written out; thus, we illustrate their behavior in the following figures.

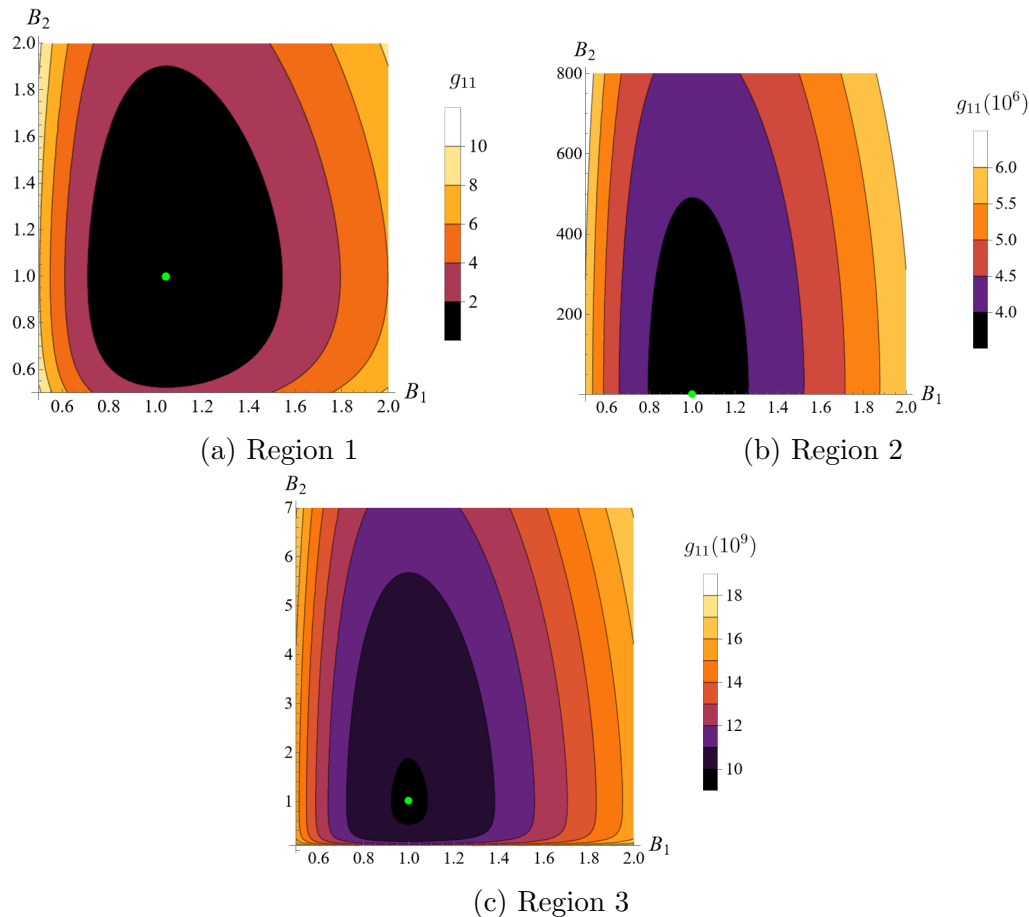


Figure 11: Component g_{11} of the tQMT for the system (77). The parameters were fixed at $X = Z = 1$ across all regions, while t was fixed as (a) $t=10$, (b) $t=5$, (c) $t=3$.

In Fig. 11, we plot the component g_{11} as a function of B_1 and B_2 , while keeping the remaining parameters fixed at $X = Z = 1$ across all regions. With this choice of parameters, the value of Y determines the region: region 1 corresponds to $Y \in (-\sqrt{2}, \sqrt{2})$; region 2 to $Y \in (-2, -\sqrt{2}) \cup (\sqrt{2}, 2)$; and region 3 to $Y \in (-\infty, -2) \cup (2, \infty)$. Taking into account this, the parameter Y is selected as $Y = 1, \sqrt{3}, 3$ for regions 1, 2, and 3, respectively. Furthermore, the parameter t is chosen differently in each region due to the distinct growth ratios observed. Some comments regarding the Fig. 11 are:

- Region 1 displays the lowest growth ratio, while region 3 exhibits the highest growth

ratio. Consequently, the choices for t were set as $t = 10, 5, 3$ for regions 1, 2, and 3, respectively.

- In region 2, the scales for B_1 and B_2 differ because B_1 is associated with the inverted normal mode (exponential behavior) while B_2 with a harmonic normal mode (trigonometric behavior).
- The three regions have a global minimum, which occurs in the neighborhood of $B_1 = B_2 = 1$ and is represented by a green point. This can be better seen in Fig. 12, where we plot the metric component g_{11} as a function of B_1 while keeping B_2 fixed at 1.

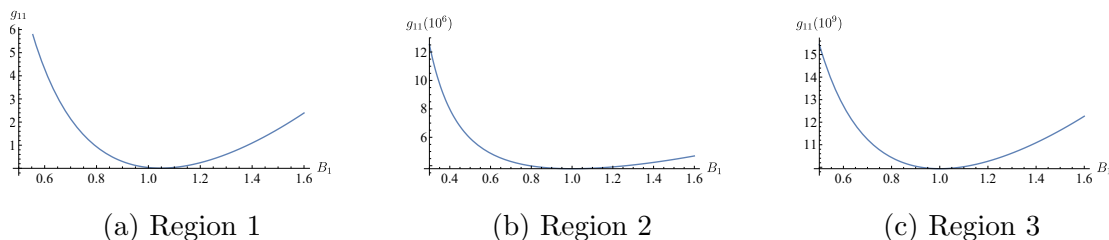


Figure 12: Component g_{11} of the tQMT for the system (77). (a) Region 1, (b) Region 2, (c) Region 3.

Similar behavior is observed for the metric components involving subscripts 1, 2, 3 (i.e., those obtained by varying the parameters X, Y, Z).

5.1.1. Scalar curvature For a more comprehensive analysis of the tQMT, we compute the scalar curvatures $\mathcal{R}[\Lambda^I, \Lambda^J]$ and $\mathcal{R}[\Lambda^I, \Lambda^J, \Lambda^K]$ associated with the 2×2 metrics $\tilde{g}[\Lambda^I, \Lambda^J]$ and 3×3 metrics $\tilde{g}[\Lambda^I, \Lambda^J, \Lambda^K]$, respectively. Once again, the expressions are too lengthy to be explicitly written out. Therefore, we illustrate their behavior graphically. The parameter values remain consistent with those used for the plots of components of the metric (see Fig. 11), except for particular choices involving t , which will be explicitly indicated in each figure.

Scalar curvature taking the parameters X and B_1

In Fig. 13, we show the scalar curvature $\mathcal{R}[X, B_1]$ as a function of the parameters B_1 and B_2 . To provide clarity, values of $\mathcal{R}[X, B_1]$ smaller than -30×10^3 and -30×10^4 are represented by white in sub-figures (a) and (b) respectively. Once again, the minimum (green point) is observed to be near $B_1 = B_2 = 1$. Also, the neighborhood of the minimum is the region where the scalar curvature exhibits the most pronounced variation. Therefore, in this neighborhood, a small change in the parameters B_1 and B_2 produces the greatest variation in the quantum system.

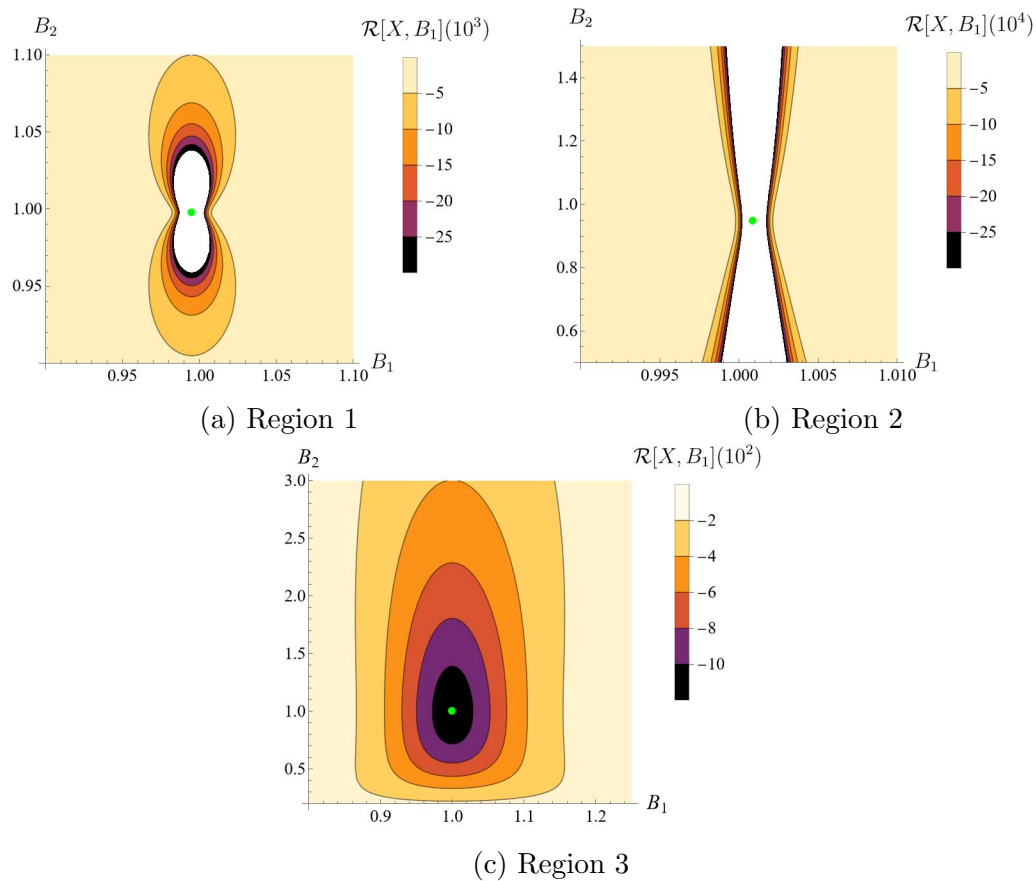


Figure 13: Scalar curvature $\mathcal{R}[X, B_1]$ as a function of the parameters B_1 and B_2 . As in Fig. 11, the parameters were fixed at $X = Z = 1$ across all regions, while t was fixed as (a) $t=10$, (b) $t=5$, (c) $t=3$.

Region 1. To observe the variation of the minimum of the scalar curvature over time, in Region 1, we cut Fig. 13a at $B_2 = 1$ and evaluate for $t = 10, 11, 12, 13$. The resulting plot is presented in Fig. 14a, where it can be observed that the minima of $\mathcal{R}[X, B_1]$ shift as t varies.

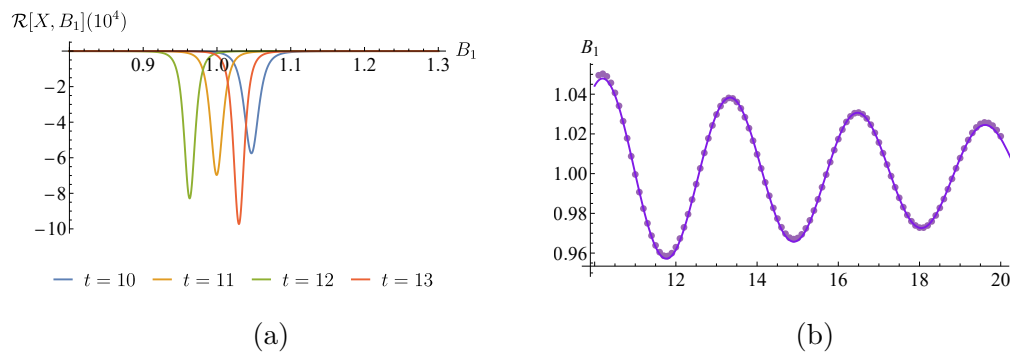


Figure 14: a) Scalar curvature $\mathcal{R}[X, B_1]$, it has an oscillating minimum around $B_1 = 1$. b) Minima points of the scalar curvature in region 1 as a function of B_1 while fixing B_2 .

In Fig. 14a, we can see that the minimum seems to oscillate around $B_1 = 1$. This oscillatory behavior can be explicitly appreciated in Fig. 14b, where we plot the value of B_1 at which the minimum of $\mathcal{R}[X, B_1]$ occurs, as a function of t , with steps of $\Delta = 0.1$. Plotting these points as a function of time reveals a damped oscillator behavior with a constant period. The function used to fit the data is

$$f(t) = c_0 \sin(c_1 + c_2 t) \exp(-c_3 t) + 1, \quad (81)$$

obtaining $c_0 = -0.098958$, $c_1 = 0.0204918$, $c_2 = -2.001312$, $c_3 = 0.071122$, with a coefficient of determination $R^2 = 0.999999$. Note that the limit $t \rightarrow \infty$ of (81) is 1, and hence the minimum of $\mathcal{R}[X, B_1]$ in the limit $t \rightarrow \infty$ occurs at $B_1 = B_2 = 1$.

A similar analysis can be carried out for fixed B_1 while varying B_2 . In Fig. 15a, we plot $\mathcal{R}[X, B_1]$ as a function of B_2 , for different values of t . Here we can see that $\mathcal{R}[X, B_1]$ exhibits a minimum for $t = 11.11, 11.12$, while it has a local maximum surrounded by two minima for $t = 11.13, 11.14, 11.15$. Then, we can identify two different patterns. The first one consists of minima in the region close to $B_2 = 1$ and the second involves a local maximum near $B_2 = 1$, surrounded by a minimum on its left and another on the right. In Fig. 15b, we plot the value of B_2 at which the minimum or local maximum of $\mathcal{R}[X, B_1]$ occurs as a function of t , with steps of $\Delta = 0.1$. Here, the red points correspond to maxima of $\mathcal{R}[X, B_1]$, while the blue ones correspond to minima. The function used to fit the data is (81), with $c_0 = -0.056185$, $c_1 = -3.124388$, $c_2 = 3.462878$, $c_3 = 0.070285$.

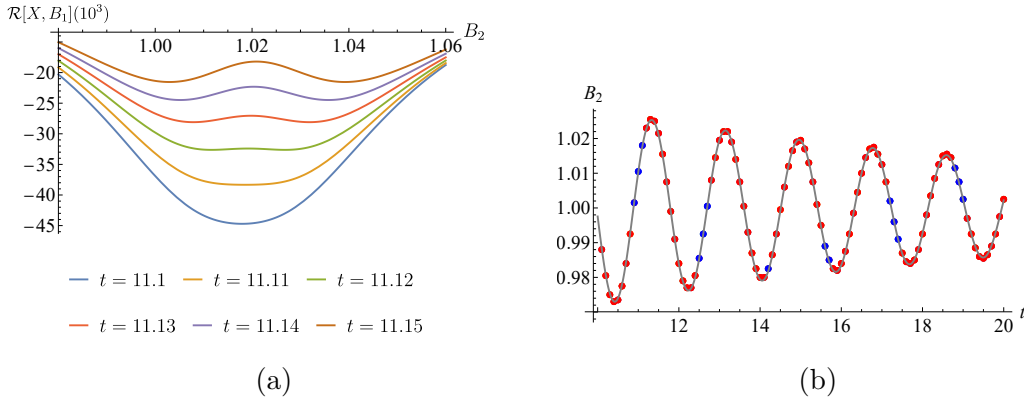


Figure 15: a) Scalar curvature $\mathcal{R}[X, B_1]$ for different times. The critical points change from minimums to local maximums. b) Extremal points of $\mathcal{R}[X, B_1]$ in region 1 as a function of B_2 while fixing B_1 .

Region 2. We examine the minima of $\mathcal{R}[X, B_1]$ when cutting Fig. 13b at $B_1 = 1$ for different times. Additionally, we study the alternative scenario where we cut Fig. 13b at $B_2 = 1$. We consider both scenarios due to the distinct behavior of the normal modes: the normal mode associated with B_1 behaves as an inverted oscillator, whereas the one associated with B_2 behaves as a harmonic oscillator. In Fig. 16a, we plot the value of B_1 at which the minimum of $\mathcal{R}[X, B_1]$ occurs, as a function of t and taking

$B_2 = 1$. The function used to fit the data in this case is

$$f(t) = c_0 \sinh(c_1 + c_2 t) \exp(-c_3 t) + 1. \quad (82)$$

In Fig. 16b, we now plot the value of B_2 at which the minimum of $\mathcal{R}[X, B_1]$ occurs, as a function of t and considering $B_1 = 1$. In this scenario, we fit the data using (81).

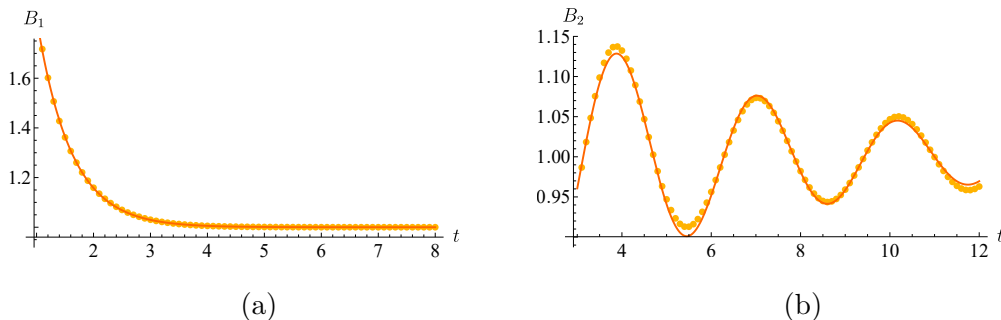


Figure 16: Minima points of the scalar curvature in region 2 as a function of: (a) B_1 while fixing B_2 , (b) B_2 while fixing B_1 .

Region 3. We analyze the minima of $\mathcal{R}[X, B_1]$ by first setting $B_1 = 1$ and then $B_2 = 1$ in Fig. 13c, for different values of t . In Figs. 17a and 17b, we plot the value of B_1 and B_2 , respectively, at which the minimum of $\mathcal{R}[X, B_1]$ occurs, as a function of t . In these scenarios, the normal modes associated with B_1 and B_2 behave as inverted oscillators, and consequently, both sets of data can be fixed using (82), as we show in Fig. 17.

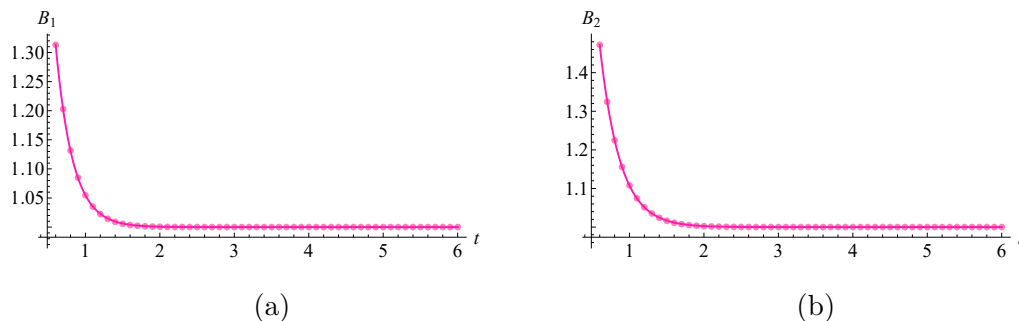


Figure 17: Extremal points of the scalar curvature $\mathcal{R}[X, B_1]$ in region 3 as a function of (a) B_1 while fixing B_2 and (b) B_2 while fixing B_1 .

Scalar curvature considering the rest of the parameters

Although the analysis was explicitly done for $\mathcal{R}[X, B_1]$, a similar examination can be carried out for the other scalar curvatures $\mathcal{R}[\Lambda^I, \Lambda^J]$. Before beginning the analysis, we introduce two new notations. First, we denote the extremal points of $\mathcal{R}[\Lambda^I, \Lambda^J]$ as x_{IJ}^* . Second, we introduce the normalized scalar curvature over Ω , defined as

$$R_{\text{norm}}[\Lambda^I, \Lambda^J] = \frac{\mathcal{R}[\Lambda^I, \Lambda^J]}{\max_{\Omega} \mathcal{R}[\Lambda^I, \Lambda^J] - \min_{\Omega} \mathcal{R}[\Lambda^I, \Lambda^J]}, \quad (83)$$

where Ω is a sub-manifold embedded in the time-parameter manifold \mathcal{M} and $\max_{\Omega} \mathcal{R}[\Lambda^I, \Lambda^J]$ ($\min_{\Omega} \mathcal{R}[\Lambda^I, \Lambda^J]$) is the maximum (minimum) of $\mathcal{R}[\Lambda^I, \Lambda^J]$ at the region Ω . We introduce R_{norm} due to the significant variation in the scales of \mathcal{R} for different parameter choices. Normalizing the scalar curvature allows a consistent comparison across different parameter choices, mitigating the effects of scale variation. Since in our plots, we fix all the parameters, excepting B_2 , the sub-manifold Ω reduces to an open interval which in our example is $(0.9, 1.05)$. There are some important remarks for the scalar curvatures, which hold for all regions:

- The scalar curvatures $\mathcal{R}[X, Z]$ and $\mathcal{R}[B_1, B_2]$ are zero.
- The scalar curvatures coming from the variation of parameters t, B_1, B_2 are time-independent.

The scalar curvatures $\mathcal{R}[\lambda^i, \lambda^j]$ (excepting $\mathcal{R}[X, Z]$ and $\mathcal{R}[B_1, B_2]$), exhibit behavior analogous to that of $\mathcal{R}[X, B_1]$, i.e., they have an extremal point in the vicinity of $B_1 = 1, B_2 = 1$. Even the extremal points appear to be very close to each other, i.e., $x_{i_1 j_1}^* \approx x_{i_2 j_2}^*$ for equal choices of parameters. This can be seen in Fig. 18 for region 1. Similar behavior occurs in regions 2 and 3.

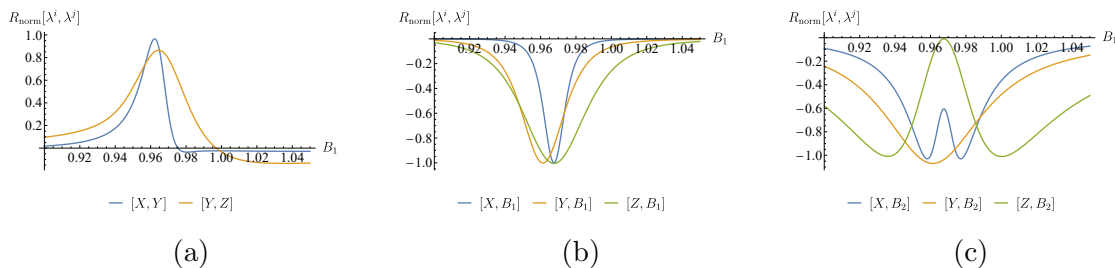


Figure 18: Normalized scalar curvatures $R_{\text{norm}}[\lambda^i, \lambda^j]$ in Region 1. They present an extremal point in the vicinity of $B_1 = 1$. The parameters were fixed at $X = Y = Z = 1$ and $t = 15$.

Now, let us analyze the remaining scalar curvatures, which are of the form $\mathcal{R}[t, \lambda^i]$. In this case, we need to distinguish between regions 1, 2, 3.

Region 1. $\mathcal{R}[t, \lambda^i]$ is singular at $B_1 = B_2 = 1$, which is a consequence of the fact that the determinant of the metric $\tilde{\mathbf{g}}[t, \lambda^i]$ is zero under this choice of parameters. This behavior can be observed in Fig. 19, where we plot $R[t, X]$ and $R[t, Y]$ as functions of B_1 . On the other hand, the scalar curvatures $\mathcal{R}[t, B_1]$ and $\mathcal{R}[t, B_2]$ result in non-continuous functions at $B_1 = B_2 = 1$, whose value depends on the order in which the limit is taken.

Regions 2 and 3. The scalar curvatures $\mathcal{R}[t, B_1]$ and $\mathcal{R}[t, B_2]$ exhibit behavior similar to that of $\mathcal{R}[\lambda^i, \lambda^j]$. However, for these scalar curvatures, their extremal point occurs precisely at $B_1 = B_2 = 1$. The extremal points are saddle points, as illustrated in Fig. 20.

After analyzing the scalar curvatures of the previous metrics, we conclude that for sufficiently large t , there is an extremal point in the neighborhood of $B_1 = B_2 = 1$. The

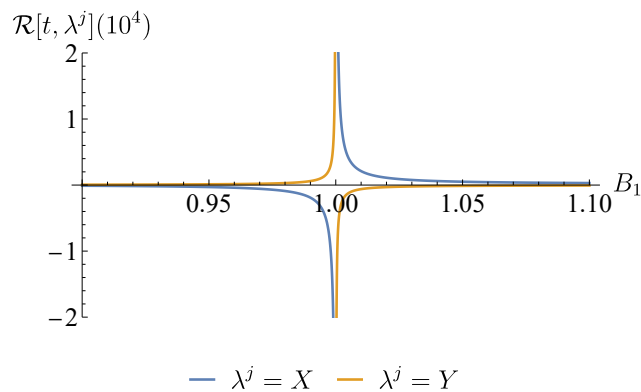


Figure 19: Scalar curvatures $R[t, X]$ and $R[t, Y]$ in region 1. They show a singularity at $B_1 = B_2 = 1$. The parameters were fixed at $B_2 = X = Y = Z = 1$, and $t = 15$. A similar behavior is observed by fixing B_1 and varying B_2 .

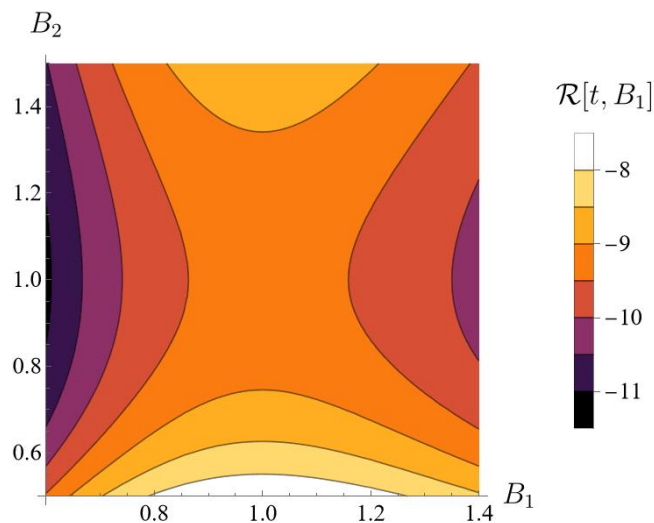


Figure 20: Scalar curvature $\mathcal{R}[t, B_1]$ in region 3. The parameters were fixed at $X = Y = Z = 1$ and $t = 3$. It has a saddle point at $B_1 = B_2 = 1$. In region 2, this curvature shows an analogous behavior.

corresponding scalar curvatures undergo the most abrupt changes around this point. Consequently, variations in the parameters B_1 and B_2 in this vicinity result in the most significant changes in the quantum system.

5.2. Purity

For systems with $N \geq 2$ degrees of freedom, we can compute additional non-trivial quantities of physical interest, especially those related to quantum entanglement. For instance, the purity μ , which is solely determined by the covariance matrix for Gaussian states [35–44]. Specifically, for a given quantum state $|\Psi(\Lambda)\rangle$, the quantum covariance

matrix $\boldsymbol{\sigma} = (\sigma_{\alpha\beta})$ is a $2N \times 2N$ matrix, with components given by

$$\sigma_{\alpha\beta} = \frac{1}{2} \langle \hat{r}_\alpha \hat{r}_\beta + \hat{r}_\beta \hat{r}_\alpha \rangle - \langle \hat{r}_\alpha \rangle \langle \hat{r}_\beta \rangle, \quad (84)$$

where $\hat{r} = \{\hat{r}_\alpha\} = (\hat{q}_1, \dots, \hat{q}_N, \hat{p}_1, \dots, \hat{p}_N)^\top$ ($\alpha, \beta = 1, \dots, 2N$) is a $2N$ -dimensional column vector and $\langle \hat{O} \rangle = \langle \Psi(\Lambda) | \hat{O} | \Psi(\Lambda) \rangle$ stands for the expectation value of an operator \hat{O} . Then, considering an k -mode Gaussian state (k denotes the number of degrees of freedom of the subsystem formed by the particles a_1, \dots, a_k of the system of N degrees of freedom) with reduced quantum covariance matrix $\boldsymbol{\sigma}^{(k)}$, the purity is

$$\mu(a_1, a_2, \dots, a_k) = \frac{1}{2^k} \frac{1}{\sqrt{\det \boldsymbol{\sigma}^{(k)}}}. \quad (85)$$

As we remark, the states (58) we consider in the present article are Gaussian, even if they have energy dispersion. To compute the purity of these states, we begin by calculating the corresponding covariance matrix. It is convenient to express the original position and momentum operators in terms of the operators corresponding to the normal modes

$$\hat{q}_a = \sum_b S_{ab} \hat{Q}_b, \quad (86a)$$

$$\hat{p}_a = \sum_b \left(S_{ab} \hat{P}_b - Y S_{ab} \hat{Q}_b \right). \quad (86b)$$

Considering a wave function of the form (58), the averages involved in the covariance matrix are

$$\langle \hat{q}_a \hat{q}_b \rangle = \frac{1}{2} (\mathbf{S} \mathbf{U}_m^{-1} \mathbf{S}^\top)_{ab}, \quad (87a)$$

$$\frac{1}{2} \langle \hat{q}_a \hat{p}_b + \hat{p}_b \hat{q}_a \rangle = \frac{1}{2} (Y \mathbf{S} \mathbf{U}_m^{-1} \mathbf{S}^\top)_{ab}, \quad (87b)$$

$$\langle \hat{p}_a \hat{p}_b \rangle = \frac{1}{2} (\mathbf{S} \mathbf{U}_m \mathbf{S}^\top + Y^2 \mathbf{S} \mathbf{U}_m^{-1} \mathbf{S}^\top)_{ab}, \quad (87c)$$

$$\langle \hat{q}_a \rangle = \langle \hat{p}_a \rangle = 0, \quad (87d)$$

where $\mathbf{U}_m = \text{diag } U_m^a$ with U_m^a being defined in (74a).

In general, to calculate the purity of a subsystem consisting of the first k oscillators, immersed in the chain of N oscillators (with $k \leq N$), we need to obtain the reduced covariance matrix in region m . This quantity is denoted by $\boldsymbol{\sigma}_m^{(k)}$, and for the present example it is given by

$$\boldsymbol{\sigma}_m^{(k)} = \begin{pmatrix} \mathbf{D}_m & -Y \mathbf{D}_m \\ -Y \mathbf{D}_m & \mathbf{L}_m + Y^2 \mathbf{D}_m \end{pmatrix}, \quad (88)$$

where \mathbf{L}_m and \mathbf{D}_m are $k \times k$ submatrices of

$$\mathbf{S}U_m\mathbf{S}^\top = \begin{pmatrix} \mathbf{L}_m & \mathbf{B}_m \\ \mathbf{B}_m^\top & \mathbf{C}_m \end{pmatrix}, \quad (89a)$$

$$\mathbf{S}U_m^{-1}\mathbf{S}^\top = \begin{pmatrix} \mathbf{D}_m & \mathbf{E}_m \\ \mathbf{E}_m^\top & \mathbf{F}_m \end{pmatrix}, \quad (89b)$$

respectively.

Using (88), the purity (85) of the k oscillators in region m turns out to be

$$\mu_m(a_1, \dots, a_k) = \frac{1}{\sqrt{\det \mathbf{L}_m \det \mathbf{D}_m}}. \quad (90)$$

We must emphasize that this purity is in general time-dependent.

In particular, for the system of two oscillators, the purity of the reduced system of one oscillator in the region m is given by

$$\mu_m(a_1) = \frac{2\sqrt{U_m^1 U_m^2}}{U_m^1 + U_m^2}, \quad (91)$$

where $m = 1, 2, 3$. The expressions for the purity $\mu_m(a_1)$, for each region m , simplifies at $B_1 = B_2 = 1$ and reduce to

$$\mu_1(a_1) = \frac{2\sqrt{\omega_1 \omega_2}}{\omega_1 + \omega_2}, \quad (92a)$$

$$\mu_2(a_1) = \frac{2\sqrt{\sec(2\alpha_1 t) \alpha_1 \omega_2}}{\sec(2\alpha_1 t) \alpha_1 + \omega_2}, \quad (92b)$$

$$\mu_3(a_1) = \frac{2\sqrt{\sec(2\alpha_1 t) \sec(2\alpha_2 t) \alpha_1 \alpha_2}}{\sec(2\alpha_1 t) \alpha_1 + \sec(2\alpha_2 t) \alpha_2}. \quad (92c)$$

Notice that for this election, $B_1 = B_2 = 1$, in region 1, the state is time-independent, and then, the purity is also time-independent. This purity coincides with the result obtained in [45].

Let us now analyze the behavior of the purity at the two bifurcations. The first bifurcation appears at the point $X - Y^2 + Za_1 = 0$, and it is the one that divides regions 1 and 2; while the second bifurcation occurs at $X - Y^2 + Za_2 = 0$, and it is the one that divides regions 2 and 3. Therefore, to analyze them, it is necessary to calculate the limit from the left and the right of the resulting purities. For region 1, this is equivalent to taking the limit $\omega_1 \rightarrow 0$ for $\mu_1(a_1)$, and $\alpha_1 \rightarrow 0$ for $\mu_2(a_1)$. Analogously, for region 2, this is equivalent to taking the limit $\omega_2 \rightarrow 0$ for $\mu_2(a_1)$, and $\alpha_2 \rightarrow 0$ for $\mu_3(a_1)$. To achieve this, we calculate U_ψ^a and U_x^a in the limit $\omega_a \rightarrow 0$ and $\alpha_a \rightarrow 0$, respectively, obtaining

$$\lim_{\omega_a \rightarrow 0} U_\psi^a \rightarrow 0, \quad (93a)$$

$$\lim_{\alpha_a \rightarrow 0} U_x^a \rightarrow 0. \quad (93b)$$

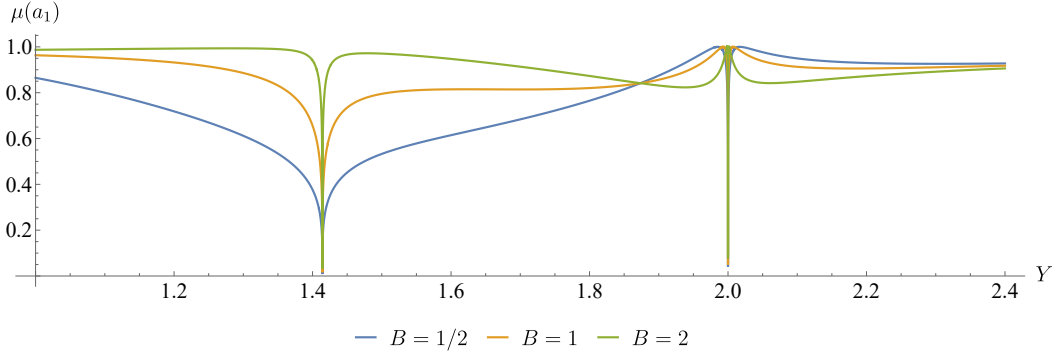


Figure 21: Purity as a function of the parameter Y . The parameters are fixed at $X = Z = 1$, with this choice of parameters, the bifurcation points are $Y = \sqrt{2}$ and $Y = 2$.

Since we are considering different frequencies, we can infer from equation (91) that the numerator approaches zero, while the denominator remains finite. Hence, the purity at the bifurcation points is zero, meaning the system is completely entangled. Also, since the left and right limits coincide, we conclude that the purity is continuous, however, a straightforward calculation shows that it is not differentiable.

For the model introduced in (77), the previous analysis can be observed in Fig. 21, where we fix the parameters $X = Z = 1$, and we consider $B_1 = B_2 = B$. With this choice of parameters, the bifurcation points are $Y = \{\sqrt{2}, 2\}$.

Let us refer back to equation (91) in region 1. Remembering that our time-dependent Gaussian functions (58) can be expressed as a Fourier series expansion of the even eigenfunctions of the harmonic oscillator as was proven (26), we can rewrite the purity as follows

$$\mu_1(a_1) = \sum_{\{2m, 2n\}} C_{\{2m, 2n\}} \int dq_1 dq_2 dx_1 dx_2 f_{2m, 2n}(x_1, x_2, q_1, q_2), \quad (94)$$

with $C_{\{2m, 2n\}} > 0$, $m = (m_1, m_2, m_3, m_4)$, $n = (n_1, n_2, n_3, n_4)$, and

$$f_{mn}(x_1, x_2, q_1, q_2) = u_{n_1, m_1}(x_1, q_2) u_{n_2, m_2}(x_1, x_2) u_{n_3, m_3}(q_1, q_2) u_{n_4, m_4}(q_1, x_2), \quad (95)$$

where u_{m_1, m_1} is the wave function of the eigenstate with energy $E_{n_1, m_1} = \omega_1(m_1 + 1/2) + \omega_2(n_2 + 1/2)$. In particular, if $m_1 = m_2 = m_3 = m_4$ and $n_1 = n_2 = n_3 = n_4$, the purity of the excited eigenstate with energy E_{n_1, m_1} is given by

$$\mu_{m_1 n_1}(a_1) := \int dq_1 dq_2 dx_1 dx_2 f_{m_1 n_1}(x_1, x_2, q_1, q_2). \quad (96)$$

In other words, equation (91) encapsulates all the information about the purity of all even states. Notably, we show that $\mu_1(a_1) \rightarrow 0$ at the bifurcation point. From equation (96), we can conclude that the purity of the reduced system of one oscillator embedded in a system of two oscillators of any even excited eigenstate at the bifurcation points is zero.

5.2.1. Equal frequencies Now, let us analyze the case where the frequencies are equal. In this case, the parameter space is divided only into 2 regions instead of 3. In the first one, both modes exhibit harmonic behavior, while in the second both modes exhibit inverted oscillator behavior.

The expression for purity remains as (91) for both regions. On the other hand, the expression for the purity at the bifurcation point conducts to an indeterminacy. Then, the analysis at this point needs to be conducted in a slightly different manner. To calculate the purity at the bifurcation point, we need the asymptotic expressions for U_ψ^a and U_χ^a for $\omega \rightarrow 0$ and $\alpha \rightarrow 0$, respectively, which are given by

$$U_\psi^a \sim B_a \omega_a, \quad (97a)$$

$$U_\chi^a \sim B_a \alpha_a. \quad (97b)$$

Using these results, the purity of a single particle of the system at the bifurcation point is given by

$$\mu_1(a_1) = \mu_2(a_1) \sim \frac{2\sqrt{B_1 B_2}}{B_1 + B_2}, \quad (98)$$

which is different from zero, unlike the previous case (different frequencies). Notice that if $B_1 = B_2$, $\mu_1(a_1) = 1$, which also holds for arbitrary parameters (X, Y, Z) . This means that the system is not entangled.

6. Conclusions

In this work, we have introduced a time-dependent extension of the quantum geometric tensor, defined on a time-parameter manifold, allowing for a full covariant description of the geometry of the parameter space in time-evolving quantum systems. By considering small variations in both time and wave function parameters, we have demonstrated that this tensor adds new temporal components, providing a new tool for systems where the quantum state is non-time-separable and/or explicitly time-dependent. In particular, we have shown that the time-time component of the tQGT is proportional to the energy dispersion of the system, whereas if we consider stationary states the tQGT reduces to the standard QGT.

The real part of the tQGT defines a time-dependent quantum metric tensor that generalizes the standard QGT of Provost and Valle, and its imaginary part provides a time-dependent (tBerry) curvature that generalizes the Berry curvature. The tQGT facilitates a better understanding of the dynamical geometric responses of quantum systems. We must emphasize that this tensor could distinguish between positive and negative average energies. Additionally, we obtained information by considering all the parameters in the wave function—which are not necessarily present in the corresponding quantum Hamiltonian—as explained in the examples. This is not possible with the standard QGT.

To illustrate a practical application of the tQGT, we have first applied our theoretical framework to a system corresponding to a harmonic/inverted oscillator, then to a time-dependent harmonic oscillator, and finally to a chain of generalized harmonic/inverted oscillators. For the harmonic/inverted oscillator system, in both cases (harmonic and inverted oscillator), we have obtained a wave function dependent on the parameter B (among other parameters), using the corresponding system's kernel from an initial wave packet. The resulting wave functions belong to the family of Gaussian states (14), for which we have found that tQMT and tBerry curvature satisfy the general properties (19). In particular, for this family of wave functions, the determinant of the tQMT is zero if the dimension of the time-parameter manifold is greater than two; for any 2-dimensional time-parameter manifolds the tQMT satisfies the Palumbo and Goldman relation and its scalar curvature is -16 , meaning that the 2-dimensional time-parameter space of these Gaussian states possesses a hyperbolic geometry.

For the harmonic oscillator regime, the analysis showed that when $B = 1$, the usual ground state of the harmonic oscillator is recovered. The expected value of the Hamiltonian was calculated, revealing that the parameter B is associated with the system's energy. The minimum energy corresponds to $B = 1$, while for other values of B , the state is a combination of all even energy eigenstates. Then, we computed the tQGT, showing its dependence on B and identifying the ground state by a minimum in specific tensor components. Additionally, we have found that the tBerry curvature is different from zero and oscillates in time, meaning that the corresponding probability distribution $\rho_H(q, t, B)$ oscillates between the two values of B with the same energy. On the other hand, we have computed the expected value of the Hamiltonian for the inverted oscillator and found that, for $B > 0$, the energy changes from negative to positive at $B = 1$. Also, at $B = 1$, all the components of the tQMT became bounded. We have observed that for large ωt , some components of the tQMT have a minimum at $B = 1$ or in the neighborhood of this value. We have also analyzed the transition region between the harmonic and inverted oscillators, focusing on the changes in the system's properties. We have found that the tQMT and tBerry curvature components obtained by varying the parameter X diverge at $X = 0$, reflecting a big change in the system.

We have studied the time-dependent harmonic oscillator to illustrate our formalism for time-dependent systems. We have shown that the Palumbo-Goldman relation is modified for this system, as shown in (54). We have found that, as g_{00} is time-independent, the energy dispersion of the system remains constant. Additionally, the system suffers a transition from an oscillator to a free particle in the limit where the time-frequency approaches zero. In our particular case, two choices for the parameters satisfy this condition. In one case, many metric components approach zero while others diverge. In contrast, in the other, there is a metric whose determinant becomes constant, i.e., parameter-independent. Similarly, in this case, some components of the tBerry curvature become constant. This demonstrates that the tQGT effectively captures the relevant physical information associated with parameter variation.

We have investigated the generalized wave functions (70), focusing on the tQMT and tBerry curvature. We have demonstrated that the determinant of the metric vanishes under specific conditions, particularly when the number of independent parameters exceeds $2N - l$, where l denotes the multiplicity of functional dependencies among the U^a and V^a functions. We then considered metrics derived from varying a subset of parameters. The scalar curvature for these metrics revealed interesting patterns, particularly for $N = 2$, where we have found $\mathcal{R}[\Lambda^{I_1}, \dots, \Lambda^{I_4}] = -32$ across different parameter sets. This pattern suggested a broader property that may extend to higher dimensions ($N > 2$). Although we did not provide formal proof, the consistency observed in multiple specific examples supports the hypothesis that the scalar curvature satisfies $\mathcal{R}[\Lambda^{I_1}, \dots, \Lambda^{I_{2N}}] = -16N$ for any set of functionally independent U^a and V^a .

One system that admits solutions of the form (70) is the generalized chain described by (65). In the case $N = 2$, we identified three distinct regions, which, in normal coordinates correspond to the following: in region 1, two harmonic oscillators; in region 2, one inverted and one harmonic oscillator; and region 3, two inverted oscillators. We computed the tQMT and tBerry curvature for the three regions. Our results revealed that the scalar curvature is highly sensitive to variations in parameters B_1 and B_2 for large values of the time parameter t . Notably, this sensitivity is pronounced near $(B_1, B_2) = (1, 1)$, indicating that the system undergoes the most abrupt changes in curvature in this region. As we have shown, this point corresponds to the ground state of the system.

On the other hand, even when the states we are working with are non-time-separable, they are Gaussian. This allowed us to derive the purity of reduced systems by analyzing the covariance matrices in the generalized chain case. We obtained the purity of the k oscillators of N in region m . We discussed in detail the case of one oscillator in a two-oscillator system across the three regions, considering different frequencies. Our study showed that at the two bifurcation points, the purity of the reduced system drops to zero, indicating complete entanglement. Furthermore, we have shown that, as the state is a combination of even excited energy-eigenstates, the purity of the reduced system of one oscillator embedded in a system of two oscillators is zero at the bifurcation points for any even excited energy-eigenstate.

To close, since the states considered here are Gaussian, we could directly compute other quantities related to quantum entanglement beyond purity. For instance, logarithmic negativity, generalized purities, Bastiaans-Tsallis entropies, and Rényi entropies [46] [42, 47–50]. Finally, it would be interesting to apply this new tool to analyze other systems, including non-Hermitian or open systems.

Acknowledgments

This work was partially supported by DGAPA-PAPIIT Grants No. IN105422 and IN114225, also by the Spanish Ministerio de Ciencia Innovación y Universidades - Agencia Estatal de Investigación grant AEI/PID2020116567GB-C22.

B. D. acknowledges support from CONAHCyT (México) No 371778. M. J. H. acknowledges support from CONAHCyT (México) No 940148. Diego Gonzalez acknowledges the financial support of Instituto Politécnico Nacional, Grant No. SIP-20240184, and the postdoctoral fellowship from Consejo Nacional de Humanidades, Ciencia y Tecnología (CONAHCyT), México.

References

- [1] Pancharatnam S 1956 *Proceedings of the Indian Academy of Sciences - Section A* **44** 247–262 URL <https://doi.org/10.1007/BF03046050>
- [2] Berry M V 1984 *Proc. R. Soc. A* **392** 45–57 ISSN 00804630 URL <http://www.jstor.org/stable/2397741>
- [3] Simon B 1983 *Phys. Rev. Lett.* **51**(24) 2167–2170 URL <https://link.aps.org/doi/10.1103/PhysRevLett.51.2167>
- [4] Aharonov Y and Anandan J 1987 *Phys. Rev. Lett.* **58**(16) 1593–1596 URL <https://link.aps.org/doi/10.1103/PhysRevLett.58.1593>
- [5] Anandan J and Aharonov Y 1988 *Phys. Rev. D* **38**(6) 1863–1870 URL <https://link.aps.org/doi/10.1103/PhysRevD.38.1863>
- [6] Samuel J and Bhandari R 1988 *Phys. Rev. Lett.* **60**(23) 2339–2342 URL <https://link.aps.org/doi/10.1103/PhysRevLett.60.2339>
- [7] Bhandari R and Samuel J 1988 *Phys. Rev. Lett.* **60**(13) 1211–1213 URL <https://link.aps.org/doi/10.1103/PhysRevLett.60.1211>
- [8] Anandan J and Aharonov Y 1990 *Phys. Rev. Lett.* **65**(14) 1697–1700 URL <https://link.aps.org/doi/10.1103/PhysRevLett.65.1697>
- [9] Provost J P and Vallee G 1980 *Commun. Math. Phys.* **76** 289–301 ISSN 1432-0916 URL <https://doi.org/10.1007/BF02193559>
- [10] Zanardi P, Giorda P and Cozzini M 2007 *Phys. Rev. Lett.* **99**(10) 100603 URL <https://link.aps.org/doi/10.1103/PhysRevLett.99.100603>
- [11] Carollo A, Valenti D and Spagnolo B 2020 *Phys. Rep.* **838** 1 – 72 ISSN 0370-1573 URL <http://www.sciencedirect.com/science/article/pii/S0370157319303655>
- [12] Dey A, Mahapatra S, Roy P and Sarkar T 2012 *Phys. Rev. E* **86**(3) 031137 URL <https://link.aps.org/doi/10.1103/PhysRevE.86.031137>
- [13] Gonzalez D, Gutiérrez-Ruiz D and Vergara J D 2020 *J. Phys. A: Math. Theor.* **53** 505305 URL <https://doi.org/10.1088/1751-8121/abc6c2>
- [14] Tong D M, Sjöqvist E, Kwek L C and Oh C H 2004 *Phys. Rev. Lett.* **93**(8) 080405 URL <https://link.aps.org/doi/10.1103/PhysRevLett.93.080405>
- [15] Chaturvedi S, Ercolessi E, Marmo G, Morandi G, Mukunda N and Simon R 2004 *The European Physical Journal C - Particles and Fields* **35** 413–423 URL <https://doi.org/10.1140/epjc/s2004-01814-5>
- [16] Leyvraz F and Heiss W D 2005 *Phys. Rev. Lett.* **95**(5) 050402 URL <https://link.aps.org/doi/10.1103/PhysRevLett.95.050402>
- [17] Caprio M, Cejnar P and Iachello F 2008 *Annals of Physics* **323** 1106–1135 ISSN 0003-4916 URL <https://www.sciencedirect.com/science/article/pii/S0003491607001042>
- [18] Anandan J and Aharonov Y 1990 *Phys. Rev. Lett.* **65**(14) 1697–1700 URL <https://link.aps.org/doi/10.1103/PhysRevLett.65.1697>
- [19] Palumbo G and Goldman N 2018 *Phys. Rev. Lett.* **121**(17) 170401 URL <https://link.aps.org/doi/10.1103/PhysRevLett.121.170401>
- [20] Freund P G and Rubin M A 1980 *Physics Letters B* **97** 233–235 ISSN 0370-2693 URL <https://www.sciencedirect.com/science/article/pii/0370269380905900>

- [21] Nepomechie R I 1985 *Phys. Rev. D* **31**(8) 1921–1924 URL <https://link.aps.org/doi/10.1103/PhysRevD.31.1921>
- [22] Barton G 1986 *Annals of Physics* **166** 322–363 ISSN 0003-4916 URL <https://www.sciencedirect.com/science/article/pii/0003491686901429>
- [23] Yuce C, Kilic A and Coruh A 2006 *Physica Scripta* **74** 114 URL <https://dx.doi.org/10.1088/0031-8949/74/1/014>
- [24] Ali T, Bhattacharyya A, Haque S S, Kim E H, Moynihan N and Murugan J 2020 *Phys. Rev. D* **101**(2) 026021 URL <https://link.aps.org/doi/10.1103/PhysRevD.101.026021>
- [25] Griffiths D 2017 *Introduction to Quantum Mechanics* (Cambridge University Press) ISBN 9781107179868 URL <https://books.google.com.mx/books?id=0h-nDAAAQBAJ>
- [26] Juárez S B, Gonzalez D, Gutiérrez-Ruiz D and Vergara J D 2023 *Physica Scripta* **98** 095106 URL <https://dx.doi.org/10.1088/1402-4896/aceb21>
- [27] Bhaduri R, Khare A, Reimann S and Tomusiak E 1997 *Annals of Physics* **254** 25–40 ISSN 0003-4916 URL <https://www.sciencedirect.com/science/article/pii/S0003491696956365>
- [28] Subramanyan V, Hegde S S, Vishveshwara S and Bradlyn B 2021 *Annals of Physics* **435** 168470 ISSN 0003-4916 special issue on Philip W. Anderson URL <https://www.sciencedirect.com/science/article/pii/S0003491621000762>
- [29] Ali T, Bhattacharyya A, Haque S S, Kim E H, Moynihan N and Murugan J 2020 *Phys. Rev. D* **101**(2) 026021 URL <https://link.aps.org/doi/10.1103/PhysRevD.101.026021>
- [30] Bhattacharyya A, Haque S S and Kim E H 2021 *Journal of High Energy Physics* **2021** 28 URL [https://doi.org/10.1007/JHEP10\(2021\)028](https://doi.org/10.1007/JHEP10(2021)028)
- [31] Bhattacharyya A, Chemissany W, Haque S S, Murugan J and Yan B 2021 *SciPost Phys. Core* **4** 002 URL <https://scipost.org/10.21468/SciPostPhysCore.4.1.002>
- [32] Lewis H R 1967 *Phys. Rev. Lett.* **18**(13) 510–512 URL <https://link.aps.org/doi/10.1103/PhysRevLett.18.510>
- [33] Dittrich W and Reuter M 2001 *Classical and Quantum Dynamics: From Classical Paths to Path Integrals* 3rd ed (Springer) ISBN 9783319582986
- [34] Chruscinski D and Jamiolkowski A 2012 *Geometric Phases in Classical and Quantum Mechanics* vol 36 (Springer Science & Business Media, New York) ISBN 9780817681760
- [35] Agarwal G S 1971 *Phys. Rev. A* **3**(2) 828–831 URL <https://link.aps.org/doi/10.1103/PhysRevA.3.828>
- [36] Holevo A S, Sohma M and Hirota O 1999 *Phys. Rev. A* **59**(3) 1820–1828 URL <https://link.aps.org/doi/10.1103/PhysRevA.59.1820>
- [37] Dodonov V V 2002 *Journal of Optics B: Quantum and Semiclassical Optics* **4** S98–S108 URL <https://doi.org/10.1088/1464-4266/4/3/362>
- [38] Paris M G A, Illuminati F, Serafini A and De Siena S 2003 *Phys. Rev. A* **68**(1) 012314 URL <https://link.aps.org/doi/10.1103/PhysRevA.68.012314>
- [39] de Gosson M 2006 *Symplectic Geometry and Quantum Mechanics* Operator Theory: Advances and Applications (Birkhäuser Basel) ISBN 9783764375751 URL <https://doi.org/10.1007/3-7643-7575-2>
- [40] Diosi L 2011 *A Short Course in Quantum Information Theory: An Approach From Theoretical Physics* Lecture Notes in Physics (Springer Berlin Heidelberg) ISBN 9783642161179 URL <https://books.google.es/books?id=w13vCAAQBAJ>
- [41] Golubeva T and Golubev Y 2014 *Journal of Russian Laser Research* **35** 47–55 URL <https://doi.org/10.1007/s10946-014-9399-2>
- [42] Serafini A 2017 *Quantum Continuous Variables: A Primer of Theoretical Methods* (CRC Press, Taylor & Francis Group) ISBN 9781482246346
- [43] de Gosson M 2019 *On the Purity and Entropy of Mixed Gaussian States* (Cham: Springer International Publishing) pp 145–158 ISBN 978-3-030-05210-2 URL https://doi.org/10.1007/978-3-030-05210-2_5
- [44] Demarie T F 2018 *European Journal of Physics* **39** 035302 URL <https://doi.org/10.1088/>

- 1361-6404/aaaad0
- [45] Díaz B, González D, Gutiérrez-Ruiz D and Vergara J D 2022 *Phys. Rev. A* **105**(6) 062412 URL <https://link.aps.org/doi/10.1103/PhysRevA.105.062412>
 - [46] Rényi A 1970 *Probability Theory* (North-Holland Amsterdam)
 - [47] Bastiaans M J 1984 *J. Opt. Soc. Am. A* **1** 711–715 URL <http://opg.optica.org/josaa/abstract.cfm?URI=josaa-1-7-711>
 - [48] Tsallis C 1988 *Journal of Statistical Physics* **52** 479–487 URL <https://doi.org/10.1007/BF01016429>
 - [49] Adesso G, Ragy S and Lee A R 2014 *Open Systems & Information Dynamics* **21** 1440001 URL <https://doi.org/10.1142/S1230161214400010>
 - [50] Díaz B, Gonzalez D, Hernández M J and Vergara J D 2023 *Phys. Rev. A* **108**(1) 012411 URL <https://link.aps.org/doi/10.1103/PhysRevA.108.012411>